

Adaptive joint distribution learning*

Damir Filipović[†] Michael Multerer[‡] Paul Schneider[§]

September 25, 2024

Abstract

We develop a new framework for estimating joint probability distributions using tensor product reproducing kernel Hilbert spaces (RKHS). Our framework accommodates a low-dimensional, normalized and positive model of a Radon–Nikodym derivative, which we estimate from sample sizes of up to several millions, alleviating the inherent limitations of RKHS modeling. Well-defined normalized and positive conditional distributions are natural by-products to our approach. Our proposal is fast to compute and accommodates learning problems ranging from prediction to classification. Our theoretical findings are supplemented by favorable numerical results.

Keywords: distribution estimation, tensor product RKHS, low-rank approximation

MSC classification: 65D05, 65D15, 62G07

JEL codes: C02, C55, C65

1 Introduction

Most empirical applications in data science have a formulation that depends on an unknown probability distribution. For instance, linear regression can be viewed as an approximation of the conditional expectation of the response variables given covariates, and classification can be viewed as the task of minimizing the unknown probability of assigning a wrong label to a variable. Both of these applications, and many others, have in common that they approximate expectations with respect to the unknown, joint stationary distribution through sample averages. If conditional distributions were available on top of sample averages, empirical researchers could assess marginal effects and even complicated questions such as causality. However, there is no canonical model for conditional distributions based only on sample averages, and the literature has accordingly developed nonparametric locally smoothed and sieve estimators [Li and Racine \[2006\]](#), [Grenander \[1981\]](#). An attractive alternative to the aforementioned models is the embedding of conditional probability distributions in reproducing kernel Hilbert spaces (RKHS). This technique has a long-standing tradition starting from covariance operators [Berlinet and Thomas-Agnan \[2004\]](#), and kernel mean embedding [Fukumizu et al. \[2004\]](#), [Smola et al. \[2007\]](#), [Song et al. \[2009, 2013\]](#). It has been shown to be a highly effective machine learning technique in finite samples, with improved properties over local approaches used in extant nonparametric regressions [Grünewälder et al. \[2012\]](#). Traditional embedding of distributions in RKHS is elegant and easily applied, and can be motivated from many different angles. For instance, the work [Grünewälder et al. \[2012\]](#) connects conditional mean embedding to the seminal vector-regression framework of [Micchelli and Pontil \[2005\]](#). In [Park and Muandet \[2020\]](#), the RKHS embedding is constructed from a measure-theoretic point of view, while [Song et al. \[2009\]](#) and [Klebanov et al. \[2020\]](#) derive it from operator theory.

*Michael Multerer gratefully acknowledges the Swiss National Science Foundation starting grant “Multiresolution methods for unstructured data” (TMSG12.211684). Paul Schneider gratefully acknowledges the Swiss National Science Foundation grant “Scenarios” (100018.189086). We thank Rohan Sen, Marc Van Uffelen for helpful comments.

[†]EPFL and Swiss Finance Institute. Email: damir.filipovic@epfl.ch

[‡]Università della Svizzera italiana. Email: michael.multerer@usi.ch

[§]Università della Svizzera italiana and Swiss Finance Institute. Email: paul.schneider@usi.ch

However, all of the above-mentioned approaches suffer from several conceptual problems. They involve assumptions concerning inverse operators that are difficult to test. Estimates of probabilities may become negative, and they are not normalized, rendering the RKHS distribution embedding framework problematic in many different situations of empirical work. A conditional covariance matrix estimated with traditional RKHS distribution embedding, for instance, is not guaranteed to be positive semidefinite, and for higher dimensions in particular is unlikely to be. Likewise, widespread classification loss functions such as the logistic loss function, become difficult to handle in the face of non-normalized and negative probabilities.

In this paper we propose a new framework to estimate a Radon–Nikodym derivative of the joint distribution with respect to the product distribution of its marginals in the spirit of [Nguyen et al. \[2010\]](#) and [Schuster et al. \[2020\]](#). We term it joint distribution learner (JDL). We construct JDL on a grid of sample points as a normalized and positive joint distribution, such that its distance to the true and unobserved population joint distribution can be decomposed additively into two parts. The first vanishes as the number of data points grows. The second constitutes the loss function that we provide in this paper, for which we also derive a representer theorem. With a tensor product RKHS this yields an optimal JDL that is bilinear in the feature maps pertaining to the RKHS used. From this representer theorem, the loss function can be minimized through a simple linear-quadratic optimization problem that can be processed through standard off-the-shelf solvers, or proximal algorithms.

JDL comes with several important advantages over the traditional embedding of distributions in RKHS. First, it enables us to represent, in particular, constants and distributions of independent random variables, that are both problematic for the traditional conditional mean embedding (CME) as shown by [Klebanov et al. \[2020\]](#). Second, JDL is normalized and positive by definition, and thus satisfies the two fundamental structural properties of probability measures. This is in contrast to the traditional distribution embedding, which is a mere projection of distributions that does not preserve these properties. To the best of our knowledge, only [Muzellec et al. \[2021\]](#) have considered these shape restrictions within embedding of distributions in RKHS. From a positive and normalized joint distribution, conditional distributions can be computed in a straightforward way. Third, we construct our Radon–Nikodym derivative directly in terms of a low-rank approximation facilitated by the pivoted Cholesky decomposition from [Bach and Jordan \[2002\]](#), [Beebe and Linderberg \[1977\]](#), [Foster et al. \[2009\]](#), [Harbrecht et al. \[2012\]](#), that allows us to control the trade-off between precision and computational tractability with a sharply controlled a-posteriori error.

Our adaptive low-rank formulation alleviates the inherent scaling limitations of RKHS modeling by crucially leveraging the tensor RKHS hypothesis. It also produces, at negligible additional computational cost, a basis transformation that diagonalizes the linear-quadratic optimization problem, making it amenable to very large data sets. A specialization to finite-dimensional hypothesis spaces, in particular polynomial RKHS with sample expectation inner products, automatically produces this basis transformation, and yields pointwise positivity constraints.

The principles behind our approach are generic, and applicable in particular also to CME. We thus provide a full description of the CME low-rank loss function, and show that it benefits from the same diagonalization as JDL, making it likewise easily solvable in applications involving several millions of data points. In addition, we propose strategies to constrain the CME optimization problem to account for normalization and positivity.

We provide numerical experiments with real and simulated data of up to 26 dimensions with up to ten million data points in prediction and classification problems. The results suggest that conditional distributions obtained from JDL perform favorably compared to CME, and even compared to more specialized setups such as kernel logistic regression. They further show computation times that allow both CME and JDL to be used in large-scale real-world applications.

The remainder of the paper is organized as follows. In [Section 2](#), we formulate the estimation problem, establish normalization and positivity as the requirements defining probability distributions, and introduce an appropriate loss function. In [Section 3](#), we introduce our tensor product hypothesis space, and prove a representer theorem subject to the structural constraints. In [Section 4](#), we develop the generic low-rank framework, that we specialize to polynomials in [Appendix B](#). In [Appendix C](#), we apply the low-rank framework to the conditional mean em-

bedding, which is then used to benchmark our method in extensive numerical experiments in Section 5. Section 6 concludes. Appendix D describes low-rank kernel logistic regression. For readability, all proofs are contained in Appendix A.

2 Problem formulation

Let X, Y be random variables taking values in some separable, complete metric spaces \mathcal{X} and \mathcal{Y} , with joint population distribution \mathbb{P} on the product space $\mathcal{Z} := \mathcal{X} \times \mathcal{Y}$ endowed with a product metric $d_{\mathcal{Z}}$. For instance, one might consider the 2-product metric $d_{\mathcal{Z}}^2 = d_{\mathcal{X}}^2 + d_{\mathcal{Y}}^2$. This minimal assumption assures the existence of conditional distributions, see Dudley [2002, Theorem 10.2], and the weak convergence of the empirical sample distributions introduced below. In practical examples, \mathcal{X} and \mathcal{Y} are subsets of the Euclidean space.

Let $z_1 = (x_1, y_1), \dots, z_n = (x_n, y_n)$ be a sample of points in \mathcal{Z} . We aim at computing a probability measure \mathbb{Q} supported on the grid $\mathcal{G} := \{(x_i, y_j) : i, j = 1, \dots, n\} \subset \mathcal{Z}$ that approximates \mathbb{P} . Such a measure \mathbb{Q} can then be used to efficiently compute various functionals, such as the conditional expectation $\mathbb{E}_{\mathbb{Q}}[f(Y)|X = x]$ of a function f on \mathcal{Y} . Any such measure \mathbb{Q} can be written as

$$\mathbb{Q} = \mathbb{Q}(h) = \frac{1}{n^2} \sum_{i,j=1}^n (1 + h(x_i, y_j)) \delta_{x_i} \otimes \delta_{y_j}, \quad (1)$$

where δ_x denotes the Dirac measure supported at x and $h: \mathcal{Z} \rightarrow \mathbb{R}$ is a function satisfying the normalization and positivity (i.e., non-negativity) properties

$$\sum_{i,j=1}^n h(x_i, y_j) = 0, \quad (2)$$

$$1 + h(x_i, y_j) \geq 0 \quad \text{for all } (x_i, y_j) \in \mathcal{G}. \quad (3)$$

In (1), the Radon–Nikodym derivative model is decomposed into the sum of a constant prior of 1 and the RKHS function h , for several reasons. Firstly, $h = 0$ is a valid choice satisfying the structural properties (2) and (3), and thus makes the feasible set non-empty regardless of the chosen (linear) hypothesis space. Secondly, $h = 0$ also coincides with the prior of independence. Below, when we estimate h in a RKHS hypothesis space \mathcal{H} with regularization, shrinking h adheres to the information-theoretic notion of minimizing mutual information. Thirdly, omitting the constant term 1 in (1) would be problematic for commonly used hypothesis spaces, such as Gaussian RKHS, that do not contain constant functions. In such cases, we can also interpret $1 + h$ as an element of the direct sum $\mathbb{R} \oplus \mathcal{H}$, where the constant is fixed to 1. More generally, one may also consider an approach based on conditionally positive definite kernels, see Wendland [2005], which then also allows to optimize the constant.

Accordingly, the marginal distributions of \mathbb{Q} on \mathcal{X} and \mathcal{Y} can be computed as

$$\mathbb{Q}_X = \frac{1}{n^2} \sum_{i,j=1}^n (1 + h(x_i, y_j)) \delta_{x_i}, \quad \mathbb{Q}_Y = \frac{1}{n^2} \sum_{i,j=1}^n (1 + h(x_i, y_j)) \delta_{y_j}, \quad (4)$$

and its conditional distributions are given by

$$\mathbb{Q}_{X|Y=y} = \frac{\sum_{i=1}^n (1 + h(x_i, y)) \delta_{x_i}}{\sum_{i=1}^n (1 + h(x_i, y))}, \quad \mathbb{Q}_{Y|X=x} = \frac{\sum_{j=1}^n (1 + h(x, y_j)) \delta_{y_j}}{\sum_{j=1}^n (1 + h(x, y_j))}. \quad (5)$$

Note that, as h is defined on \mathcal{Z} , the measures $\mathbb{Q}_{X|Y=y}$ and $\mathbb{Q}_{Y|X=x}$ naturally extend to all $x \in \mathcal{X}$ and $y \in \mathcal{Y}$, albeit they may become signed measures, and the denominators in (5) may become zero and may cause numerical issues.

We denote by $\hat{\mathbb{P}} := \frac{1}{n} \sum_{i=1}^n \delta_{z_i} = \frac{1}{n} \sum_{i=1}^n \delta_{x_i} \otimes \delta_{y_i}$ the empirical distribution with marginals $\hat{\mathbb{P}}_X := \frac{1}{n} \sum_{i=1}^n \delta_{x_i}$ and $\hat{\mathbb{P}}_Y := \frac{1}{n} \sum_{i=1}^n \delta_{y_i}$. The latter differ from \mathbb{Q}_X and \mathbb{Q}_Y in general, as the following elementary lemma shows.

Lemma 2.1. *We have*

(i) $\mathbb{Q}_X = \hat{\mathbb{P}}_X$ if and only if $\sum_{i':x_{i'}=x_i} \sum_{j=1}^n h(x_{i'}, y_j) = 0$ for all $i = 1, \dots, n$.

(ii) $\mathbb{Q}_Y = \hat{\mathbb{P}}_Y$ if and only if $\sum_{j':y_{j'}=y_j} \sum_{i=1}^n h(x_i, y_{j'}) = 0$ for all $j = 1, \dots, n$.

To assess how far $\mathbb{Q}(h)$ is from the population distribution \mathbb{P} , we decompose this distance into two parts, the distance between $\hat{\mathbb{P}}$ and \mathbb{P} , and the distance between $\mathbb{Q}(h)$ and $\hat{\mathbb{P}}$. For the first part, we recall the definition of the dual-bounded Lipschitz metric measuring the distance between two probability measures P, Q on \mathcal{Z} given by

$$\beta(P, Q) := \sup_{\|f\|_{BL} \leq 1} \left| \int_{\mathcal{Z}} f dP - \int_{\mathcal{Z}} f dQ \right|. \quad (6)$$

Herein, we set

$$\|f\|_{BL} := \sup_{z \in \mathcal{Z}} |f(z)| + \sup_{z_1 \neq z_2} \frac{|f(z_1) - f(z_2)|}{d_{\mathcal{Z}}(z_1, z_2)},$$

see [Dudley \[2002, Section 11.3\]](#) for the definitions. In fact, β metrizes weak convergence of probability measures on \mathcal{Z} . Therefore, $\beta(\hat{\mathbb{P}}, \mathbb{P}) \rightarrow 0$ a.s. for $n \rightarrow \infty$ whenever z_1, \dots, z_n is an i.i.d. sample drawn from \mathbb{P} , see for instance [Dudley \[2002, Theorem 11.4.1\]](#). Hence, for any $\epsilon_1 > 0$ there exists n large enough such that¹

$$\beta(\hat{\mathbb{P}}, \mathbb{P}) \leq \epsilon_1. \quad (7)$$

For the second part, we note that $d\mathbb{Q}(h) = (1 + h) d(\hat{\mathbb{P}}_X \otimes \hat{\mathbb{P}}_Y)$ for any function h . This suggests that we measure the distance between $\mathbb{Q}(h)$ and $\hat{\mathbb{P}}$, similarly to (6), by the squared *worst case loss*

$$\mathcal{E}(h) := \sup_{\|f\|_{L^2_{\hat{\mathbb{P}}_X \otimes \hat{\mathbb{P}}_Y}} \leq 1} \left| \int_{\mathcal{Z}} f d\hat{\mathbb{P}} - \int_{\mathcal{Z}} f d\mathbb{Q}(h) \right|^2.$$

Note that $\hat{\mathbb{P}} = \mathbb{Q}(\hat{h})$ for any function $\hat{h} : \mathcal{Z} \rightarrow \mathbb{R}$ such that $1 + \hat{h}(x_i, y_j) = n \delta_{ij}$. Henceforth, we fix such a function \hat{h} . This implies that we can write

$$\mathcal{E}(h) = \sup_{\|f\|_{L^2_{\hat{\mathbb{P}}_X \otimes \hat{\mathbb{P}}_Y}} \leq 1} \left| \langle f, \hat{h} - h \rangle_{L^2_{\hat{\mathbb{P}}_X \otimes \hat{\mathbb{P}}_Y}} \right|^2 = \|\hat{h} - h\|_{L^2_{\hat{\mathbb{P}}_X \otimes \hat{\mathbb{P}}_Y}}^2.$$

Adding these two components, we arrive at the following result.

Lemma 2.2. *Assume that (7) holds and let h be such that (2) and (3) hold. Then the dual-bounded Lipschitz distance between $\mathbb{Q}(h)$ and the population distribution \mathbb{P} is bounded by $\beta(\mathbb{Q}(h), \mathbb{P}) \leq \epsilon_1 + \mathcal{E}(h)^{1/2}$.*

Lemma 2.2 states that, for large enough n such that (7) holds, it remains to find h such that $\mathcal{E}(h)$ is small, so that $\mathbb{Q}(h)$ is close to the population distribution \mathbb{P} . In this paper, we will choose h optimally from a separable RKHS \mathcal{H} on \mathcal{Z} . Specifically, we solve the convex optimization problem

$$\underset{h \in \mathcal{H} \text{ s.t. (2), (3)}}{\text{minimize}} \left\{ \mathcal{E}(h) + \lambda \|h\|_{\mathcal{H}}^2 \right\}, \quad (8)$$

for some regularization parameter $\lambda > 0$.

¹In the case of an absolutely continuous distribution \mathbb{P} on $\mathcal{Z} = \mathbb{R}^d$, this may require n of the order ϵ_1^{-d} , see [Dudley \[1969, Proposition 2.1\]](#).

3 Representer theorem

We assume a tensor product RKHS $\mathcal{H} = \mathcal{H}_X \otimes \mathcal{H}_Y$ as hypothesis space for the function $h: \mathcal{Z} \rightarrow \mathbb{R}$, where \mathcal{H}_X and \mathcal{H}_Y are separable RKHS on \mathcal{X} and \mathcal{Y} , respectively. The associated reproducing kernels are denoted by k_X and k_Y , respectively. The reproducing kernel k of \mathcal{H} satisfies $k((x, y), (x', y')) = k_X(x, x')k_Y(y, y')$, $x, x' \in \mathcal{X}$, $y, y' \in \mathcal{Y}$.

In what follows, we refer to the row vectors of canonical feature maps as

$$\Phi_X(\cdot) := [k_X(x_1, \cdot), \dots, k_X(x_n, \cdot)], \quad \Phi_Y(\cdot) := [k_Y(y_1, \cdot), \dots, k_Y(y_n, \cdot)], \quad (9)$$

and to the associated kernel matrices by $\mathbf{K}_X := [\Phi_X(x_i)]_{i=1}^n$, $\mathbf{K}_Y := [\Phi_Y(y_i)]_{i=1}^n$.

For any function h on \mathcal{Z} we define the matrix of function values with respect to the grid \mathcal{G} as $h|_{\mathcal{G}} := [h(x_j, y_i)]_{i,j=1}^n \in \mathbb{R}^{n \times n}$. That is, rows and columns of $h|_{\mathcal{G}}$ correspond to y_i and x_j , respectively, i.e., $(h|_{\mathcal{G}})_{ij} = h(x_j, y_i)$. We denote by $\mathbf{1} \in \mathbb{R}^n$ the column vector consisting of 1's and by $\mathbf{E} := \mathbf{1}\mathbf{1}^\top \in \mathbb{R}^{n \times n}$ the matrix consisting of 1's.

The following representer theorem states that the solution to (8) lies in the subspace spanned by the functions $\Phi_{X,i} \otimes \Phi_{Y,j}$, $i, j = 1, \dots, n$, in \mathcal{H} .

Theorem 3.1. *The solution to (8) is of the form*

$$h = h(\mathbf{H}) := \Phi_Y(\cdot)\mathbf{H}\Phi_X(\cdot)^\top, \quad (10)$$

for some $\mathbf{H} \in \mathbb{R}^{n \times n}$. That is, $h|_{\mathcal{G}} = \mathbf{K}_Y\mathbf{H}\mathbf{K}_X$. The linear constraints (2) and (3) accordingly read

$$\mathbf{1}^\top \mathbf{K}_Y \mathbf{H} \mathbf{K}_X \mathbf{1} = 0, \quad (11)$$

$$\mathbf{E} + \mathbf{K}_Y \mathbf{H} \mathbf{K}_X \geq \mathbf{0}, \text{ element-wise}, \quad (12)$$

and problem (8) is equivalent to the n^2 -dimensional optimization problem

$$\underset{\mathbf{H} \in \mathbb{R}^{n \times n} \text{ s.t. (11), (12)}}{\text{minimize}} \quad \mathcal{R}_\lambda(\mathbf{H}), \quad (13)$$

where the regularized objective function is defined by

$$\begin{aligned} \mathcal{R}_\lambda(\mathbf{H}) := & \frac{1}{n^2} \text{trace}(\mathbf{H}^\top \mathbf{K}_Y \mathbf{K}_Y \mathbf{H} \mathbf{K}_X \mathbf{K}_X) - \frac{2}{n} \text{trace}(\mathbf{K}_Y \mathbf{H} \mathbf{K}_X) \\ & + \frac{2}{n^2} \text{trace}(\mathbf{1}^\top \mathbf{K}_Y \mathbf{H} \mathbf{K}_X \mathbf{1}) + \lambda \text{trace}(\mathbf{H}^\top \mathbf{K}_Y \mathbf{H} \mathbf{K}_X). \end{aligned} \quad (14)$$

With constraint (11) imposed, the third term on the right hand side of (14) is identically equal to zero. We nevertheless include it in the sections below to consider also unconstrained versions of (13), without the constraints (11) and (12).

4 Adaptive low-rank approximation

Problem (13) is of dimension n^2 , which may become computationally too demanding for large sample sizes n . We therefore propose an efficient low-rank representation of the kernel matrix that provides an approximation of the full problem the error of which we quantify below in Lemma 4.1 together with 4.4. Specifically, we consider here an adaptive low-rank approach based on the pivoted Cholesky decomposition for the kernel matrices \mathbf{K}_X and \mathbf{K}_Y . We first present an algorithm that calculates a bi-orthogonal basis transformation concurrently with the pivoted Cholesky decomposition in Section 4.1. We then propose an additional rotation into a basis that is orthogonal in both \mathcal{H} and $L_{\hat{\mathbb{P}}_X \otimes \hat{\mathbb{P}}_Y}^2$ in Section 4.2. This double orthogonality diagonalizes the quadratic terms in objective (14), greatly facilitating its optimization. In Appendix B, we investigate the JDL with a finite-dimensional polynomial basis, that, on top of its inherent low-rank nature, also allows for pointwise positivity through a sum-of-squares constraint.

4.1 Pivoted Cholesky decomposition and bi-orthogonal basis

In this section, we propose Algorithm 1 that computes an incomplete Cholesky decomposition $\mathbf{L}_m \mathbf{L}_m^\top$ of any given symmetric and positive semidefinite matrix \mathbf{K} , concurrently with a bi-orthogonal basis transformation \mathbf{B}_m . The basis transformation is an essential byproduct to efficiently solving the low-rank approximation of the constrained optimization problem (13) at large scale.

Algorithm 1 Pivoted Cholesky decomposition

input: symmetric and positive semidefinite matrix $\mathbf{K} \in \mathbb{R}^{n \times n}$, tolerance $\varepsilon > 0$
output: low-rank approximation $\mathbf{L}_m \in \mathbb{R}^{n \times m}$ with $\mathbf{K} \approx \mathbf{L}_m \mathbf{L}_m^\top$,
matrix $\mathbf{B}_m \in \mathbb{R}^{n \times m}$ with $\mathbf{B}_m^\top \mathbf{L}_m = \mathbf{I}_{m \times m}$

- 1: Initialization: set $m := 1$, $\mathbf{d}_0 := \text{diag}(\mathbf{K})$, $\mathbf{L}_0 := []$, $\mathbf{B}_0 := []$,
- 2: **while** $\|\mathbf{d}_{m-1}\|_1 > \varepsilon$
- 3: determine $p_m := \arg \max_{1 \leq i \leq n} d_{m-1,i}$
- 4: compute

$$\boldsymbol{\ell}_m := \frac{1}{\sqrt{d_{m-1,p_m}}} (\mathbf{K} - \mathbf{L}_{m-1} \mathbf{L}_{m-1}^\top) \mathbf{e}_{p_m}$$

- 5: compute

$$\mathbf{b}_m := \frac{1}{\sqrt{d_{m-1,p_m}}} (\mathbf{I} - \mathbf{B}_{m-1} \mathbf{L}_{m-1}^\top) \mathbf{e}_{p_m}$$

- 6: set $\mathbf{L}_m := [\mathbf{L}_{m-1}, \boldsymbol{\ell}_m]$, $\mathbf{B}_m := [\mathbf{B}_{m-1}, \mathbf{b}_m]$
 - 7: set $\mathbf{d}_m := \mathbf{d}_{m-1} - \boldsymbol{\ell}_m \odot \boldsymbol{\ell}_m$, where \odot denotes the element-wise product
 - 8: set $m := m + 1$
-

Based on the choice of the pivot element in line 3 of Algorithm 1, we obtain different well known low-rank approximations of the kernel matrix. The presented Algorithm 1 employs a greedy strategy and always removes the largest entry of the Schur complement, cp. Harbrecht et al. [2012]. Alternatively, one may choose a random pivot element, resulting in the well known Nyström approximation, cp. Williams and Seeger [2000]. Finally, a maximal reduction of the trace is achieved by selecting the pivot corresponding to the column of the Schur complement with the largest Euclidean norm, cp. Higham [1996]. This comes at the cost of assembling the full kernel matrix, and quickly becomes inefficient for larger sample sizes. Hence, we opt here for the current version, since it is rather cost-efficient and provides rigorous a posteriori error bounds for the approximation. To decouple the matrix approximation error from its size, we shall consider a relative error in our numerical experiments. That is, in line 2, we replace the *absolute* tolerance ε by $\varepsilon \text{trace}(\mathbf{K})$, for a *relative* tolerance ε .

Employing the associativity of the matrix product in lines 4 and 5 of Algorithm 1, it is easy to see that the cost of computing $\boldsymbol{\ell}_m$ and \mathbf{b}_m is of order $\mathcal{O}(mn)$ each. Hence, the cost of performing m steps of Algorithm 1 is of cost $\mathcal{O}(m^2n)$. Moreover we emphasize that the full matrix \mathbf{K} never needs to be computed. It is rather sufficient to provide the pivot columns and the diagonal.

Validity of Algorithm 1 is substantiated by the following theorem.

Theorem 4.1. *For any tolerance $\varepsilon > 0$, Algorithm 1 computes $n \times m$ -matrices \mathbf{B}_m and \mathbf{L}_m with $m \leq \text{rank } \mathbf{K}$ such that $\mathbf{K} - \mathbf{L}_m \mathbf{L}_m^\top$ is positive semidefinite and*

$$\text{trace}(\mathbf{K} - \mathbf{L}_m \mathbf{L}_m^\top) \leq \varepsilon, \quad (15)$$

$$\text{Im } \mathbf{B}_m = \text{span}\{\mathbf{e}_{p_1}, \dots, \mathbf{e}_{p_m}\}, \quad (16)$$

$$\mathbf{B}_m^\top \mathbf{L}_m = \mathbf{I}_{m \times m}, \quad (17)$$

$$\mathbf{K} \mathbf{B}_m = \mathbf{L}_m. \quad (18)$$

Below we employ Algorithm 1 to also speed up the computations of the conditional mean embedding considered in Grünwälder et al. [2012] resulting in a computational cost of $\mathcal{O}(nm^2)$,

a memory cost of $\mathcal{O}(m^2)$, cp. (16), and an evaluation cost of $\mathcal{O}(m^2)$. Alternatively, other established low-rank approaches known in literature, such as FALKON, see Meanti et al. [2020], or EigenPro3, see Abedsoltan et al. [2023], may be used. By employing a matrix-free iterative approach, FALKON and EigenPro3 (with exact projection) achieve a computational cost of $\mathcal{O}(nm)$ per iteration. This is an improvement over the cost of $\mathcal{O}(nm^2)$ of Algorithm 1, if less than m iterations are required to achieve a satisfactory accuracy. However, the evaluation cost of CME in the matrix-free setting is $\mathcal{O}(nm)$, which is larger than the $\mathcal{O}(m^2)$, which we attain. Thus, matrix-free approaches such as FALKON or EigenPro3 may be computationally favorable if only a few evaluations are required.

4.2 Double-orthogonal basis

Building on the bi-orthogonal basis transformation \mathbf{B}_m , we can define an additional rotation that diagonalizes the quadratic parts of the regularized objective function (14), greatly simplifying the linearly constrained quadratic optimization problem. From a spectral decomposition $\mathbf{V}_m \mathbf{\Lambda}_m \mathbf{V}_m^\top = \mathbf{L}_m^\top \mathbf{L}_m$ that is of cost $\mathcal{O}(m^3)$, we can compute

$$\mathbf{Q}_m := \mathbf{B}_m \mathbf{V}_m. \quad (19)$$

Applying Algorithm 1 and the additional rotation (19) separately to both \mathbf{K}_X and \mathbf{K}_Y , yields matrices \mathbf{Q}_X and \mathbf{Q}_Y of dimension $n \times m_X$ and $n \times m_Y$, respectively. We then approximate the n^2 -dimensional optimization problem (13) by parametrizing the argument through $\tilde{\mathbf{H}} = \mathbf{Q}_Y \tilde{\mathbf{H}} \mathbf{Q}_X^\top$ for some $m_Y \times m_X$ -dimensional matrix $\tilde{\mathbf{H}}$. Inserting this parametrization into \mathcal{R}_λ , and using the identities

$$\begin{aligned} \text{trace}(\mathbf{H}^\top \mathbf{K}_Y \mathbf{H} \mathbf{K}_X) &= \text{trace}(\tilde{\mathbf{H}}^\top \mathbf{Q}_Y^\top \mathbf{K}_Y \mathbf{Q}_Y \tilde{\mathbf{H}} \mathbf{Q}_X^\top \mathbf{K}_X \mathbf{Q}_X) = \text{trace}(\tilde{\mathbf{H}}^\top \tilde{\mathbf{H}}), \\ \text{trace}(\mathbf{H}^\top \mathbf{K}_Y \mathbf{K}_Y \mathbf{H} \mathbf{K}_X \mathbf{K}_X) &= \text{trace}(\tilde{\mathbf{H}}^\top \mathbf{\Lambda}_Y \tilde{\mathbf{H}} \mathbf{\Lambda}_X), \end{aligned}$$

gives the low-rank regularized objective function on $\mathbb{R}^{m_Y \times m_X}$ by

$$\begin{aligned} \tilde{\mathcal{R}}_\lambda(\tilde{\mathbf{H}}) := \mathcal{R}_\lambda(\mathbf{Q}_Y \tilde{\mathbf{H}} \mathbf{Q}_X^\top) &= \frac{1}{n^2} \text{trace}(\tilde{\mathbf{H}}^\top \mathbf{\Lambda}_Y \tilde{\mathbf{H}} \mathbf{\Lambda}_X) - \frac{2}{n} \text{trace}(\mathbf{L}_Y \mathbf{V}_Y \tilde{\mathbf{H}} \mathbf{V}_X^\top \mathbf{L}_X^\top) \\ &\quad + \frac{2}{n^2} \text{trace}(\mathbf{1}^\top \mathbf{L}_Y \mathbf{V}_Y \tilde{\mathbf{H}} \mathbf{V}_X^\top \mathbf{L}_X^\top \mathbf{1}) + \lambda \text{trace}(\tilde{\mathbf{H}}^\top \tilde{\mathbf{H}}). \end{aligned}$$

The linear constraints (11) and (12) read in terms of $\tilde{\mathbf{H}}$ as

$$\mathbf{1}^\top \mathbf{L}_Y \mathbf{V}_Y \tilde{\mathbf{H}} \mathbf{V}_X^\top \mathbf{L}_X^\top \mathbf{1} = 0, \quad (20)$$

$$\mathbf{E} + \mathbf{L}_Y \mathbf{V}_Y \tilde{\mathbf{H}} \mathbf{V}_X^\top \mathbf{L}_X^\top \geq \mathbf{0}, \text{ element-wise, respectively.} \quad (21)$$

In summary, this leads to the low-rank optimization problem

$$\begin{aligned} &\text{minimize} && \tilde{\mathcal{R}}_\lambda(\tilde{\mathbf{H}}). \\ &\tilde{\mathbf{H}} \in \mathbb{R}^{m_Y \times m_X} \text{ s.t.} && (20), (21) \end{aligned} \quad (22)$$

Combining this with (10), the low-rank approximated solution to (8) is then given by

$$\tilde{\mathbf{h}} = \mathbf{\Psi}_Y(\cdot) \tilde{\mathbf{H}} \mathbf{\Psi}_X(\cdot)^\top \quad (23)$$

for the rotated low-rank row vectors of basis functions $\mathbf{\Psi}_X(\cdot) := \mathbf{\Phi}_X(\cdot) \mathbf{Q}_X$ and $\mathbf{\Psi}_Y(\cdot) := \mathbf{\Phi}_Y(\cdot) \mathbf{Q}_Y$. That is, $\tilde{\mathbf{h}}$ lies in the $m_X m_Y$ -dimensional subspace

$$\tilde{\mathcal{H}} := \text{span}\{\mathbf{\Psi}_{X,i} \otimes \mathbf{\Psi}_{Y,j} : i = 1, \dots, m_X, j = 1, \dots, m_Y\} \quad (24)$$

in \mathcal{H} . As claimed above, the additional rotation forms simultaneously orthogonal sets in \mathcal{H}_X and $L_{\mathbb{P}_X}^2$, and \mathcal{H}_Y and $L_{\mathbb{P}_Y}^2$, respectively. This can be seen from the following identities,

$$[\langle \mathbf{\Psi}_{X,i}, \mathbf{\Psi}_{X,j} \rangle_{\mathcal{H}_X}]_{i,j=1}^{m_X} = \mathbf{I}, \quad [\langle \mathbf{\Psi}_{Y,i}, \mathbf{\Psi}_{Y,j} \rangle_{\mathcal{H}_Y}]_{i,j=1}^{m_Y} = \mathbf{I} \quad (25)$$

and

$$\left[\langle \mathbf{\Psi}_{X,i}, \mathbf{\Psi}_{X,j} \rangle_{L_{\mathbb{P}_X}^2} \right]_{i,j=1}^{m_X} = \frac{1}{n} \mathbf{\Lambda}_X, \quad \left[\langle \mathbf{\Psi}_{Y,i}, \mathbf{\Psi}_{Y,j} \rangle_{L_{\mathbb{P}_Y}^2} \right]_{i,j=1}^{m_Y} = \frac{1}{n} \mathbf{\Lambda}_Y,$$

for the two diagonal eigenvalue matrices $\mathbf{\Lambda}_X$ and $\mathbf{\Lambda}_Y$.

4.3 Positivity constraint tightenings

In this section, we discuss the positivity constraint (12), and describe two different tightenings. The first, computationally intensive, tightening is built upon bounded kernels, and ensures pointwise positivity. The second is a computationally attractive single-inequality tightening of (12). The choice between these two types of positivity models, pointwise versus data-almost-sure can be motivated through weighing the trade off between empirical and computational needs and capacities. In the sections below, we exclusively use the second kind, that we find to be empirically attractive with only very few constraint violations out-of-sample. In Appendix B, we furthermore describe pointwise positivity through a sum-of-squares constraint. We suggest to use pointwise positivity when the number of data points is small and the probability to evaluate far away from the observed data points is large.

4.3.1 Pointwise positivity for bounded kernels

Assuming bounded kernels on both \mathcal{X} and \mathcal{Y} , we have that $\phi_{X,j}(z)\phi_{Y,i}(z) \in [a_{i,j}, b_{i,j}]$, for $z \in \mathcal{Z}$, for some finite $a_{i,j} < b_{i,j}$, for all $i = 1, \dots, m_Y, j = 1, \dots, m_X$. Accordingly, we define the hyperrectangle $C := \prod_{i=1, \dots, m_Y; j=1, \dots, m_X} [a_{i,j}, b_{i,j}]$ and the convex set $\mathcal{C} := \{\mathbf{H} \in \mathbb{R}^{m_Y \times m_X} \mid \min_{\mathbf{x} \in C} \mathbf{x}^\top \text{vec}(\mathbf{H}) + 1 \geq 0\}$, where $\text{vec}(\cdot)$ denotes the operator that concatenates the columns of a matrix into a column vector. Clearly, for any $\mathbf{H} \in \mathcal{C}$ we have $1 + h(\mathbf{H}) \geq 0$ pointwise in \mathcal{Z} , which implies (3), or equivalently (12). Decomposing $\text{vec}(\mathbf{H}) = \mathbf{h}^+ - \mathbf{h}^-$, with $\mathbf{h}^-, \mathbf{h}^+ \succeq \mathbf{0}$, we derive the following equivalent characterization of \mathcal{C} .

Lemma 4.2 (Non-negativity for bounded kernels). *Set $\mathbf{a} := \text{vec}([a_{i,j}]_{i=1, \dots, m_Y, j=1, \dots, m_X})$ and $\mathbf{b} := \text{vec}([b_{i,j}]_{i=1, \dots, m_Y, j=1, \dots, m_X})$. We have that $\mathbf{H} \in \mathcal{C}$ if and only if*

$$\mathbf{a}^\top \mathbf{h}^+ - \mathbf{b}^\top \mathbf{h}^- + 1 \geq 0. \quad (26)$$

In this case, (12) is satisfied.

The above pointwise tightening could also be applied to the positivity constraint (21) expressed in the rotated basis functions.

4.3.2 Single-inequality tightening

The positivity constraint (21), and (12) and its pointwise tightening (26), are sets of $n \times n$ inequalities. For large n , as in our experiments below, this may become computationally prohibitive. We thus replace it with a single-inequality tightening based on the maxima and minima of the columns of the matrices $\mathbf{L}_X \mathbf{V}_X$ and $\mathbf{L}_Y \mathbf{V}_Y$, respectively, i.e.,

$$\begin{aligned} \bar{\mathbf{c}}_{X,j} &:= \max_{i=1, \dots, n} [\mathbf{L}_X \mathbf{V}_X]_{i,j}, & \underline{\mathbf{c}}_{X,j} &:= \min_{i=1, \dots, n} [\mathbf{L}_X \mathbf{V}_X]_{i,j}, & j &= 1, \dots, m_X, \\ \bar{\mathbf{c}}_{Y,j} &:= \max_{i=1, \dots, n} [\mathbf{L}_Y \mathbf{V}_Y]_{i,j}, & \underline{\mathbf{c}}_{Y,j} &:= \min_{i=1, \dots, n} [\mathbf{L}_Y \mathbf{V}_Y]_{i,j}, & j &= 1, \dots, m_Y. \end{aligned}$$

For any real number a , we denote by $a^+ := \max\{a, 0\}$ and $a^- := -\min\{a, 0\}$ its positive and negative parts, respectively. Define the $m_Y \times m_X$ matrices $\underline{\mathbf{C}}$ and $\bar{\mathbf{C}}$ by

$$\underline{\mathbf{C}}_{i,j} := (\underline{\mathbf{c}}_{Y,i})^+ (\underline{\mathbf{c}}_{X,j})^+ + (\bar{\mathbf{c}}_{Y,i})^- (\bar{\mathbf{c}}_{X,j})^- - \max\{(\bar{\mathbf{c}}_{Y,i})^+ (\underline{\mathbf{c}}_{X,j})^-, (\underline{\mathbf{c}}_{Y,i})^- (\bar{\mathbf{c}}_{X,j})^+\}, \quad (27)$$

$$\bar{\mathbf{C}}_{i,j} := \max\{(\bar{\mathbf{c}}_{Y,i})^+ (\bar{\mathbf{c}}_{X,j})^+, (\underline{\mathbf{c}}_{Y,i})^- (\underline{\mathbf{c}}_{X,j})^-\} - (\bar{\mathbf{c}}_{Y,i})^- (\underline{\mathbf{c}}_{X,j})^+ - (\underline{\mathbf{c}}_{Y,i})^+ (\bar{\mathbf{c}}_{X,j})^-. \quad (28)$$

Then replace $n \times n$ positivity constraints (21) by the single constraint

$$1 + \text{trace}(\underline{\mathbf{C}}^\top \tilde{\mathbf{H}}^+) - \text{trace}(\bar{\mathbf{C}}^\top \tilde{\mathbf{H}}^-) \geq 0, \quad (29)$$

where we define the $m_Y \times m_X$ matrices $\tilde{\mathbf{H}}^+$ and $\tilde{\mathbf{H}}^-$ to consist of the positive parts $\tilde{H}_{i,j}^+$ and negative parts $\tilde{H}_{i,j}^-$, respectively. The following lemma asserts that this is a tightening indeed.

Lemma 4.3. *If $\tilde{\mathbf{H}}$ satisfies (29) then it also satisfies (21).*

Evidently, the cost of computing (27) and (28) is much lower than for the right hand side of (36) and (37), which requires $\mathcal{O}(n^2)$, in terms of given matrices $\mathbf{L}_Y \mathbf{V}_Y$ and $\mathbf{L}_X \mathbf{V}_X$.

4.4 Elementary approximation error bounds

Note that the low-rank approximated solution $\tilde{h} \in \tilde{\mathcal{H}}$ in (23) is different from the orthogonal projection in \mathcal{H} , say $h_{\tilde{\mathcal{H}}}$, of the solution h in (10) on the subspace $\tilde{\mathcal{H}}$ in (24). The next result gives elementary lower and upper bounds on the low-rank approximation error, $\|h - \tilde{h}\|_{\tilde{\mathcal{H}}}^2$, in terms of $h_{\tilde{\mathcal{H}}}$ and the tolerance ε . This illustrates the trade-off between computational tractability and precision. We denote by $\|\cdot\|_F$ the Frobenius norm.

Lemma 4.4. *Let h from (10) and \tilde{h} from (23) denote the solutions to (8) and (22), respectively, solved with low-rank tolerances $\text{trace}(\mathbf{K}_X - \mathbf{L}_X \mathbf{L}_X^\top) < \varepsilon$ and $\text{trace}(\mathbf{K}_Y - \mathbf{L}_Y \mathbf{L}_Y^\top) < \varepsilon$. Then the orthogonal projection of h on $\tilde{\mathcal{H}}$ is of the form $h_{\tilde{\mathcal{H}}} = \Psi_Y(\cdot) \mathbf{H}_{\tilde{\mathcal{H}}} \Psi_X^\top(\cdot)$ with coefficient matrix given by*

$$\mathbf{H}_{\tilde{\mathcal{H}}} = \arg \min_{\mathbf{H}' \in \mathbb{R}^{m_Y \times m_X}} \|h - \Psi_Y(\cdot) \mathbf{H}' \Psi_X^\top(\cdot)\|_{\tilde{\mathcal{H}}}^2 = \mathbf{V}_Y^\top \mathbf{L}_Y^\top \mathbf{H} \mathbf{L}_X \mathbf{V}_X. \quad (30)$$

Moreover, we have

$$\|\mathbf{H}_{\tilde{\mathcal{H}}} - \tilde{\mathbf{H}}\|_F^2 \leq \|h - \tilde{h}\|_{\tilde{\mathcal{H}}}^2 \leq \varepsilon \|\mathbf{H}\|_F^2 (\text{trace} \mathbf{K}_X + \text{trace} \mathbf{K}_Y) + \|\mathbf{H}_{\tilde{\mathcal{H}}} - \tilde{\mathbf{H}}\|_F^2.$$

5 Numerical experiments

To assess the performance of the proposed JDL, we conduct numerical prediction and classification experiments with both real and simulated data. We consider conditional second-moment matrices, as well as binary classification as test tasks. Both types of numerical experiments crucially rely upon positivity and normalization of the implied probability measures, as any conditional second moment matrix ought to be positive semidefinite, and the classification probabilities ought to take values in the unit interval. These are testable structural features, that we evaluate for different sample sizes and dimensions, along with suitable loss functions. As a natural benchmark for our proposed JDL, we consider *conditional mean embedding* (CME) proposed by Song et al. [2009] and Grünewälder et al. [2012], as well as kernel logistic regression (KLR) for binary classification.

CME's construction also facilitates a tensor product RKHS, $\mathcal{H} = \mathcal{H}_X \otimes \mathcal{H}_Y$. However, through convenient cancellations, see Footnote 3, \mathcal{H}_Y does not explicitly feature other than as a nuisance space that is merely used for function evaluation in its original definition. In particular, the kernel matrix \mathbf{K}_Y never needs to be computed or used in any way. However, for large sample sizes CME becomes computationally intractable.

To put conditional distribution embedding on comparable computational footing with JDL proposed in this paper, we develop a low-rank version for CME in Appendix C, along with the structural constraints. For KLR we develop the corresponding low-rank representation in Appendix D. Low-rank CME is computationally tractable also for large-scale problems, but it comes at the price of introducing a low-rank version of \mathbf{K}_Y that is not present in the full unconstrained $n \times n$ CME problem. This leaves us with the choice between the necessity of validating only one kernel parameter, but not being able to process large data sets, or having to validate two kernel parameters for large data sets. In our numerical experiments we opt for the latter in order to process large n data sets, as already $n = 1000$ poses a formidable matrix inversion problem.

We use two types of hypothesis spaces for JDL, a Gaussian RKHS, to which we refer to as JDL, and a polynomial RKHS with order $q = 4$, as described in Section B, referred to as JPDL. CME and KLR are implemented with Gaussian RKHS. For all experiments, we implement Algorithm 1 (Theorem 4.1) with absolute tolerance ε in line 2 (in (15)) replaced by $\varepsilon \text{trace}(\mathbf{K})$, for a relative tolerance ε .

We consider both structurally constrained, and unconstrained versions of JDL, JPDL, and CME. For JDL the constraints are incorporated through (20) and (29), for JPDL through (20) and (39). CME is less suitable to normalization, as (47) shows that it amounts to n restrictions even in the low-rank case. Clearly, this constraint is impractical for large n , and infeasible in general, unless the dimension $m_X m_Y$ of the argument is greater than n . We therefore only use the

weaker constraint demanding unconditional normalization (51). Positivity for CME, described in (49), could in principle be imposed through the same one-equation tightening (29) as for JDL. However, this constraint turns out to be infeasible for all examples and parameterizations developed in this section. We therefore use the weaker constraint of unconditional positivity from (52), that is feasible for most parameterizations and examples below.

5.1 Conditional moment matrices

Simulated data may reveal the behaviour of the embeddings with respect to the sample size, as well as the low-rank approximation in a controlled environment. We consider two types of distributions, Gaussian and uniform, as conditional expectations are readily available for both.

To obtain draws from multivariate Gaussian distributions with varying degrees of dependency, we first generate $j = 1, \dots, 100$ random correlation matrices of dimension $2d$, where $d = 3$, following the algorithm described in Archakov and Hansen [2021]. Assuming zero means and unit standard deviations for simplicity, we subsequently sample from the corresponding multivariate Gaussian distribution data sets $z_1^{(j)}, \dots, z_n^{(j)}$ of size $n = 10^3, 10^4, 10^5, 10^6, 10^7$, for each of the $j = 1, \dots, 100$ correlation matrices. We split each of the data sets into a training set of size $n_{\text{train}} = 4n/5$ and a validation set of size $n/5$ to validate the kernel and regularization hyperparameters. To test the distributions out-of-sample, we draw for each of the $j = 1, \dots, 100$ correlation matrices additional $n_{\text{test}} = 5,000$ data points from the same distribution that generated the training and validation sets. We additionally investigate very small data sets of size $n = 50, 100, 200$ with respect to structural behavior of the moment matrices, where each of the realizations $z_i^{(j)} = (u_{i,1}^{(j)}, (u_{i,1}^{(j)} + u_{i,2}^{(j)})/2, \dots, (u_{i,1}^{(j)} + \dots + u_{i,2d}^{(j)})/(2d))$, with $u_{i,1}^{(j)}, \dots, u_{i,2d}^{(j)}$ i.i.d. draws from a uniform distribution on the unit interval.

Second-moment matrices play an important role in many applications involving regression-type models and quadratic forms of optimization problems that are convex only if they are positive semidefinite. If they are generated by probability measures, they are always positive semidefinite. Consequently, a non positive semidefinite second-moment matrix indicates that it has not been generated by a bona fide probability measure. Ubiquitous across many fields, second-moment matrices thus constitute an important test case. We therefore keep track of the properties of the resulting conditional moment matrices for each of the simulations, on top of how well they predict squares of random variables.

Corresponding to the task of estimating conditional second-moment matrices, we introduce the test function $\mathcal{T} : \mathcal{Y} \mapsto \mathbb{R}^{d \times d}$, $\mathcal{T}(y) := [y_1, \dots, y_d]^\top [y_1, \dots, y_d]$.

Writing \mathcal{M} as placeholder for the models JDL (joint distribution learning, Gaussian RKHS), JDPL (joint distribution learning, polynomial RKHS), CME (conditional mean embedding, Gaussian RKHS), we use the second-moment squared loss function

$$\frac{1}{n_{\text{test}}} \sum_{i=1}^{n_{\text{test}}} \frac{\left\| \mathbb{E}^{\mathbb{Q}_{Y|X=x_i^{\text{test},j}}} [\mathcal{T}(Y)] - \mathbb{E}_{\theta_j, \mathcal{M}}^{\mathbb{Q}_{Y|X=x_i^{\text{test},j}}} [\mathcal{T}(Y)] \right\|_F^2}{\left\| \mathbb{E}^{\mathbb{Q}_{Y|X=x_i^{\text{test},j}}} [\mathcal{T}(Y)] \right\|_F^2} \quad (31)$$

to (validate) test the models, where $x_1^{\text{test},j}, \dots, x_{n_{\text{test}}}^{\text{test},j}$ denotes the test sample (for the validation this is replaced by the validation sample), and θ_j the (to be) validated hyperparameters pertaining to model \mathcal{M} , in experiment j .

We compare accuracy, structural preservation, and speed of the methods. For each of the criteria, we compare the mean and 5% and 95% quantiles of the sampling distribution of the second-moment squared loss (31) over the $j = 1, \dots, 100$ runs of the competing models, considering both the unconstrained and the constrained versions. We consider unconstrained versions to gauge how much the structural restrictions tilt the embeddings away from the statistical optimum. Unconstrained problems are solved on two, the constrained problems on ten Intel Xeon 2.3 GHz processors. For $n \leq 10^5$, low-rank algorithm 1 is applied to the kernel matrices with relative tolerance $\varepsilon = 10^{-3}$, for $n = 10^6$ with $\varepsilon = 10^{-2}$, and for $n = 10^7$ with $\varepsilon = 10^{-1}$. JPDL features $\varepsilon = 0$ by construction. Larger relative tolerances for larger n are chosen to keep the computation times and memory requirements low also for large data sets. In the one-dimensional

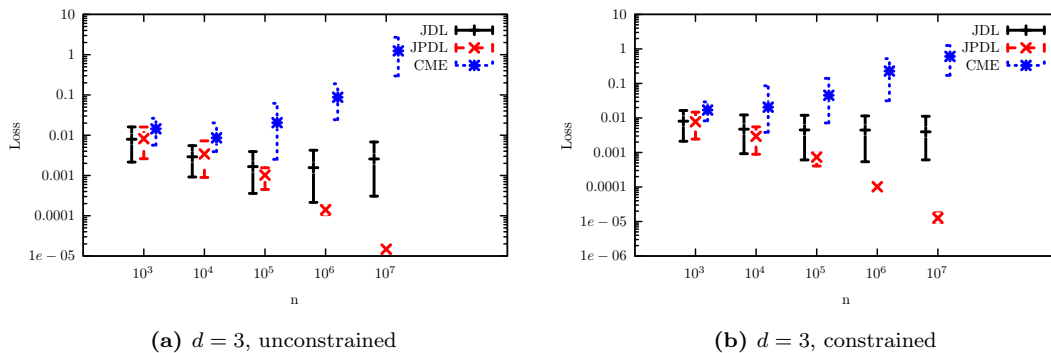


Figure 1: Second-moment squared loss. The panels show loss function (31) evaluated over $n_{\text{test}} = 5,000$ samples for the joint distribution learner (JDL), the polynomial joint distribution learner (JPDL), and the conditional mean embedding (CME) on the y -axis. The x -axis shows the number n of data points used for training and validation. The data are generated from a mean-zero, unit standard deviation multivariate Gaussian distribution with covariance matrix sampled from the algorithm proposed by Archakov and Hansen [2021]. For $n \leq 10^5$, low-rank algorithm 1 is applied to the kernel matrices with tolerance $\varepsilon = 10^{-3}$, for $n = 10^6$ with $\varepsilon = 10^{-2}$, and for $n = 10^7$ with $\varepsilon = 10^{-1}$. JPDL features $\varepsilon = 0$.

case, we furthermore investigate the behaviour of the embeddings with varying relative tolerance ε when n grows large.

Figure 1 shows the second-moment squared loss (31) as a function of the data sample size n for $d = 1, 2, 3$. JPDL dominates JDL, which again dominates CME. All models except JPDL may incur losses with increasing n , which is due to the increasing relative tolerance level ε , and is most pronounced for CME. Indeed, Figure 2 illustrates the trade-off between n and ε for CME in the one-dimensional case. Panel 2b shows that losses may become larger with increasing n , if also ε is increased. At least in the one-dimensional case this is not so for JDL: Panel 2a indicates it to be largely robust to changes in the tolerance. Figure 1 further indicates that CME losses are particularly pronounced for higher dimensions.

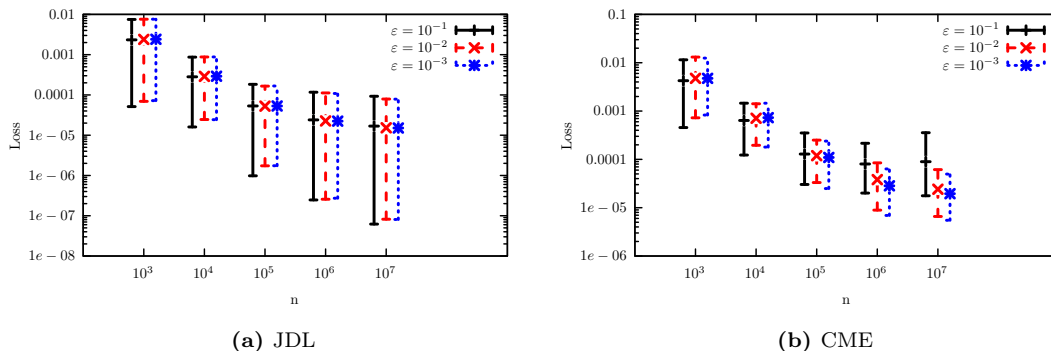


Figure 2: Low-rank tolerance and data size. The panels show loss function (31) evaluated over $n_{\text{test}} = 5,000$ samples for the joint distribution learner (JDL) and the conditional mean embedding (CME) on the y -axis. The x -axis shows the number n of data points used for training and validation. The data are generated from a mean-zero, unit standard deviation multivariate Gaussian distribution with covariance matrix sampled from the algorithm proposed by Archakov and Hansen [2021]. Tolerances are indicated in the figures.

Figure 3 shows the worst-case normalization deviation,

$$\max_{i=1, \dots, n_{\text{test}}; j=1, \dots, 100} \left| \mathbb{E}_{\theta_j, \mathcal{M}}^{\mathbb{Q}_{Y|X=x_i^{\text{test},j}}} [1] - 1 \right|,$$

over all experiments. By construction, JDE and JPDE are normalized also without constraints.

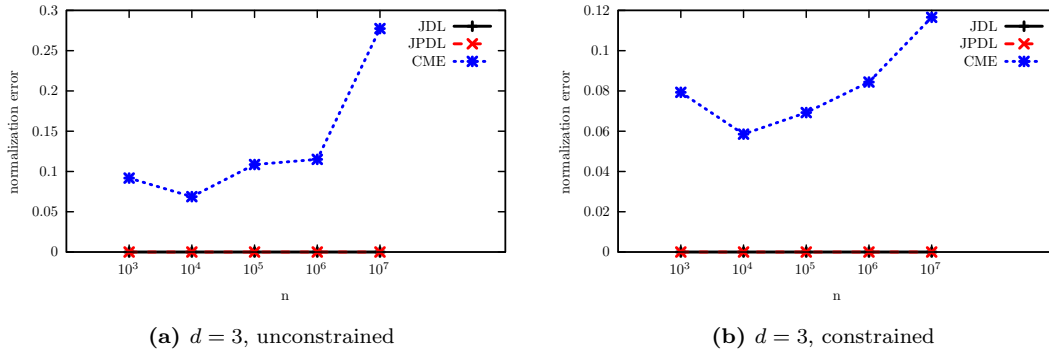


Figure 3: Normalization error. The panels show the maximal normalization error over $n_{\text{test}} = 5,000$ samples for the unconstrained joint distribution learner (JDL), the polynomial joint distribution learner (JPDL), and the conditional mean embedding (CME) on the y -axis. The x -axis shows the number n of data points used for training and validation. The data are generated from a mean-zero, unit standard deviation multivariate Gaussian distribution with covariance matrix sampled from the algorithm proposed by Archakov and Hansen [2021]. For $n \leq 10^5$, low-rank algorithm 1 is applied to the kernel matrices with tolerance $\varepsilon = 10^{-3}$, for $n = 10^6$ with $\varepsilon = 10^{-2}$, and for $n = 10^7$ with $\varepsilon = 10^{-1}$. JPDL features $\varepsilon = 0$.

On the contrary, CME exhibits sizable normalization errors that are inversely related to sample size, and comove with the precision of the low-rank approximation. Figure 4 illustrates this pattern in one dimension: at a relative tolerance of $\varepsilon = 10^{-3}$ the worst-case normalization error decreases monotonically with n . For both $\varepsilon = 10^{-2}$ and $\varepsilon = 10^{-1}$ the normalization error is lowest at $n = 10^5$ data points, but then increases only slightly with n for $\varepsilon = 10^{-2}$, while it grows quite substantially for $\varepsilon = 10^{-1}$. Figure 3 shows that structural constraints mitigate normalization errors.

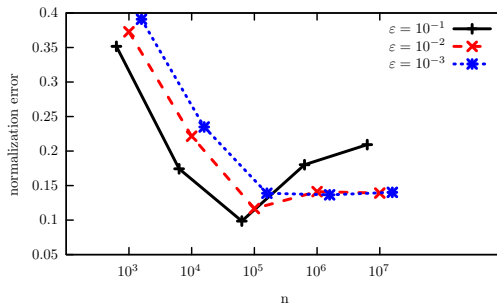


Figure 4: CME normalization error, low-rank and data size trade-off. The panel shows the maximal normalization error over $n_{\text{test}} = 5,000$ samples for the conditional mean embedding (CME). The x -axis shows the number n of data points used for training and validation. The data are generated from a mean-zero, unit standard deviation multivariate Gaussian distribution for $d = 3$, with covariance matrix sampled from the algorithm proposed by Archakov and Hansen [2021]. Tolerances are indicated in the legend.

Next, we estimate for each simulation run $j = 1, \dots, 100$ the probability that the estimated moment matrix fails to be positive semidefinite up to machine precision,

$$\frac{1}{n_{\text{test}}} \sum_{t=1}^{n_{\text{test}}} \left(1 - \mathbb{1} \left(\mathbb{E}_{\theta_j, \mathcal{M}}^{\mathbb{Q}_{Y|X=x_t^{\text{test},j}}} [\mathcal{T}(Y)] \succeq 0 \right) \right),$$

where $\mathbb{1}$ denotes the indicator function and, as before, \mathcal{M} is a placeholder for the model under consideration. Figure 5 shows that all methods but CME in the three-dimensional case perform

well with respect to this criterion. Similarly to the results on losses and normalization, CME encounters problems when the relative tolerance ε of the low-rank approximation becomes too large. Figure 6 shows positivity and normalization errors for uniformly distributed small data sets with $n = 50, 100, 200$. Here, JPDL shows an increased occurrence of positivity violations, in particular for $n = 50$, while JDL outperforms CME, which however only for $n = 50$ suggests a probability of 5% of generating moment matrices that are not symmetric positive semidefinite, and zero for more data points. Normalization errors of CME are smaller than those generated by Gaussian data. For heavy-tailed data generated from a Cauchy distribution, Figure 7 shows that the positivity errors are increased in general for $n = 50, 100, 200$. In addition to the positivity of covariance matrices, Panel 7b shows the percentage of negative realizations of the model-implied Radon-Nikodym derivative. Both panels indicate that JDL exhibits the smallest violations by far.

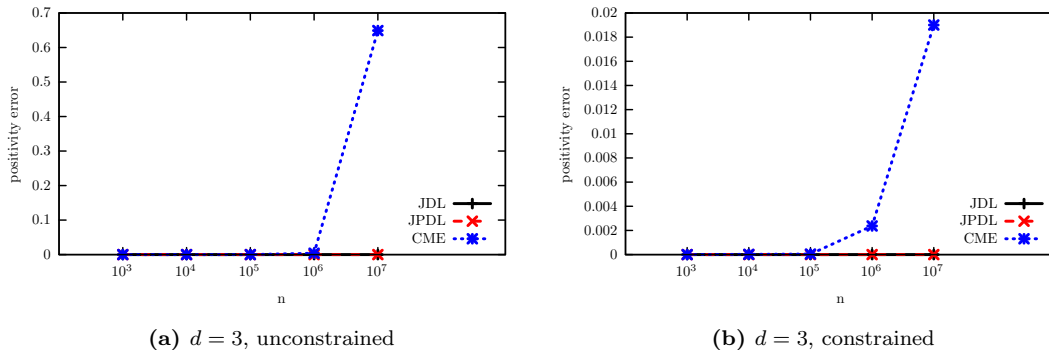


Figure 5: Positivity error. The panels show the percentage of second-moment matrices over $n_{\text{test}} = 5,000$ samples that fail to be positive semidefinite for the joint distribution learner (JDL), the polynomial joint distribution learner (JPDL), and the conditional mean embedding (CME) on the y -axis. The x -axis shows the number n of data points used for training and validation. The data are generated from a mean-zero, unit standard deviation multivariate Gaussian distribution with covariance matrix sampled from the algorithm proposed by Archakov and Hansen [2021]. For $n \leq 10^5$, low-rank algorithm 1 is applied to the kernel matrices with tolerance $\varepsilon = 10^{-3}$, for $n = 10^6$ with $\varepsilon = 10^{-2}$, and for $n = 10^7$ with $\varepsilon = 10^{-1}$. JPDL features $\varepsilon = 0$.

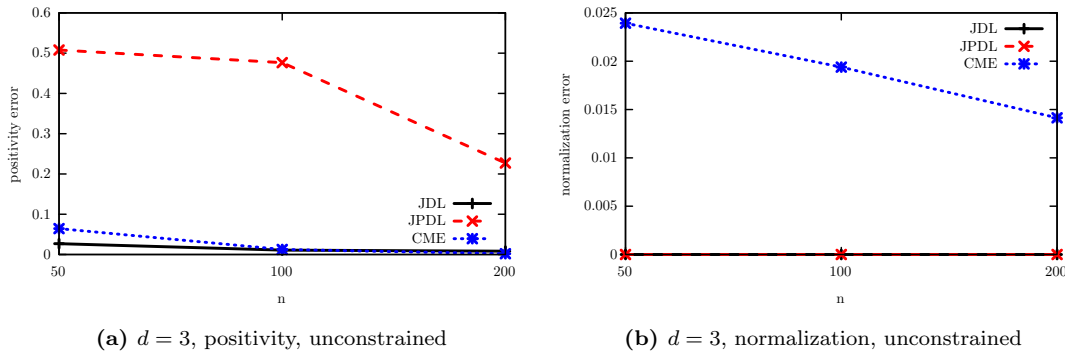


Figure 6: Positivity and normalization error for small uniform data sets. The panels show the percentage of second-moment matrices over $n_{\text{test}} = 5,000$ samples that fail to be positive semidefinite for the joint distribution learner (JDL), the polynomial joint distribution learner (JPDL), and the conditional mean embedding (CME) on the y -axis. The x -axis shows the number n of data points used for training and validation. The data are generated as $(U_1, (U_1 + U_2)/2, \dots, (U_1 + \dots + U_6)/6)$, where U_1, \dots, U_6 are i.i.d. draws from the uniform distribution on the unit interval. Low-rank Algorithm 1 is applied to the kernel matrices with tolerance $\varepsilon = 10^{-6}$. JPDL features $\varepsilon = 0$.

Figure 8 compares the methods with respect to their computational speeds, which is measured as the time needed to solve for the optimal coefficients, and to evaluate $n_{\text{test}} = 5,000$ conditional

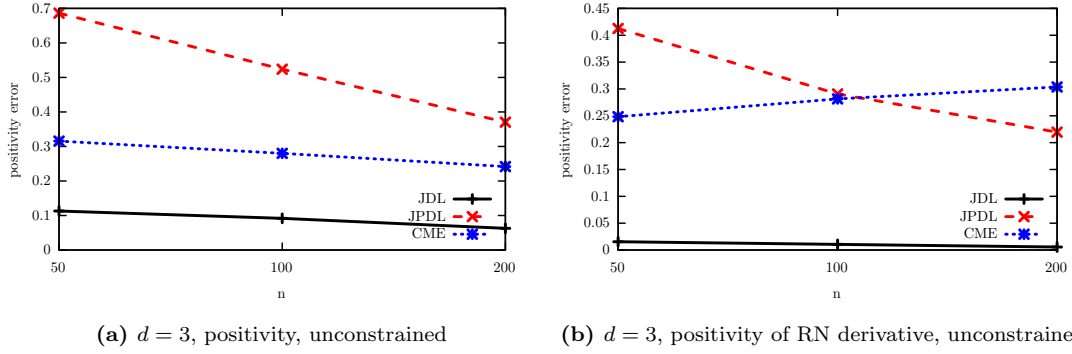


Figure 7: Positivity error for small Cauchy data sets. The left panel shows the percentage of second-moment matrices that fail to be positive semidefinite, the right panel the percentage of a negative Radon-Nikodym derivative over $n_{\text{test}} = 5,000$ samples for the joint distribution learner (JDL), the polynomial joint distribution learner (JPDL), and the conditional mean embedding (CME, evaluated against indicator functions as $\mathbf{I}\mathbf{F}\Phi_X^\top(\cdot)$ in (43) on the y-axis). The x-axis shows the number n of data points used for training and validation. The data are generated as $(C_1, (C_1+C_2)/2, \dots, (C_1+\dots+C_6)/6)$, where C_1, \dots, C_6 are i.i.d. draws from the Cauchy distribution with location zero and scale 0.1. Low-rank Algorithm 1 is applied to the kernel matrices with tolerance $\varepsilon = 10^{-6}$. JPDL features $\varepsilon = 0$.

expectations. It shows that in the unconstrained case, JDL and CME are not distinguishable from each other. JPDL is orders of magnitudes faster in the unconstrained case compared to JDL and CME. The unconstrained solution, which is available in closed form, is only minimally faster than the constrained version. The exponentially growing dimension of the subspace to describe the s.o.s. cone (39) in d of JPDL becomes a significant computational burden for JPDL for higher-dimensional problems. For instance, in the case $d = 3$ and $q = 4$, the cone is described through a symmetric positive semidefinite matrix of dimension $\binom{6+4}{6} = 210$. As a consequence, JPDL outperforms the other methods only for large sample sizes n .

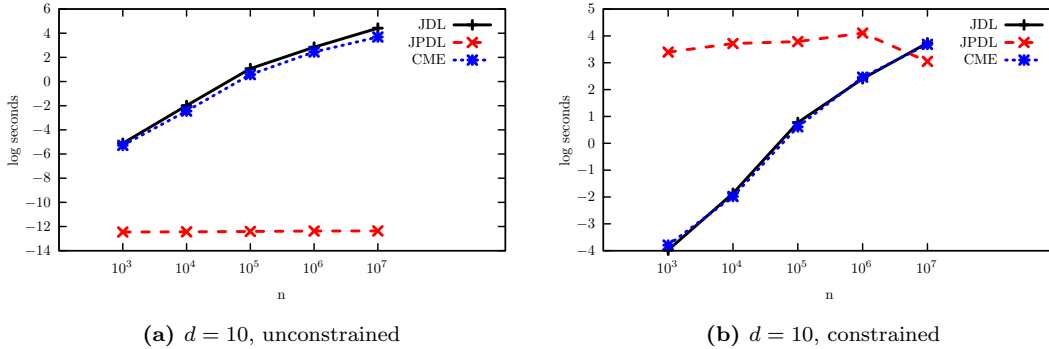


Figure 8: Second-moment computation speed. The panels show the running time of solving for the optimal coefficients, and calculating conditional expectations using $n_{\text{test}} = 5,000$ samples for the joint distribution learner (JDL), the polynomial joint distribution learner (JPDL), and the conditional mean embedding (CME) on the y-axis. The x-axis shows the number n of data points used for training and validation. The data are generated from a mean-zero, unit standard deviation multivariate Gaussian distribution with covariance matrix sampled from the algorithm proposed by Archakov and Hansen [2021]. For $n \leq 10^5$, low-rank algorithm 1 is applied to the kernel matrices with tolerance $\varepsilon = 10^{-3}$, for $n = 10^6$ with $\varepsilon = 10^{-2}$, and for $n = 10^7$ with $\varepsilon = 10^{-1}$. JPDL features $\varepsilon = 0$.

5.2 Binary classification

To assess the competing methods in a real-world application, we consider in this section a binary classification problem using portfolio excess return data from Fama-French. The data set

contains more than 25,000 daily excess returns $z_t = [z_{t,1}, \dots, z_{t,25}]$ of 25 portfolios. We are interested in predicting the conditional probability that the excess return aggregated over the first $d \leq 25$ portfolios $y_t := \sum_{i=1}^d z_{t,i} \in \mathcal{Y} = \mathbb{R}$ falls below a given threshold q , given preceding portfolio returns $x_t := [z_{t-1,1}, \dots, z_{t-1,d}] \in \mathcal{X} = \mathbb{R}^d$. In other words, the probability that the indicator $\mathcal{I}_q(y_t) := \mathbb{1}(y_t \leq q)$ equals 1.

Similarly to the previous experiment, we subsample $j = 1, \dots, 100$ data sets $z_1^{(j)}, \dots, z_n^{(j)}$ of sizes $n = 1,000, 5,000, 10,000, 20,000$, of varying numbers of portfolios $d \in \{1, 5, 10, 25\}$. We use $n_{\text{train}} = 4n/5$ data points for training and the remaining $n/5$ to validate the kernel and regularization hyperparameters. To test the models out-of-sample, we draw for each of the $j = 1, \dots, 100$ samples additional 5,000 data points without replacement from the remaining data set, which are not used for training or validation.

For each experiment (j, n, d) , we set $q = q(j, n, d)$ to be the 1%-quantile of the empirical distribution of the aggregated portfolio excess returns $y_t^{(j)} = \sum_{i=1}^d z_{t,i}^{(j)}$, $t = 1, \dots, n$.

We use the logistic loss function to validate and test all models. The logistic loss function (and others), require normalized and positive probabilities from the classifier. Since some of the models tested are neither pointwise normalized nor positive, we adapt the logistic loss function, here written for the test data, as

$$-\frac{1}{n_{\text{test}}} \sum_{t=1}^{n_{\text{test}}} \mathcal{I}_q(y_t^{\text{test},j}) \log \min \left(1, \max \left(\mathbb{E}_{\theta_j, \mathcal{M}}^{\mathbb{Q}_{Y|X=x_t^{\text{test},j}}} [\mathcal{I}_q(Y)], \eta \right) \right) - \frac{1}{n_{\text{test}}} \sum_{t=1}^{n_{\text{test}}} (1 - \mathcal{I}_q(y_t^{\text{test},j})) \log \max \left(\eta, \min \left(1 - \mathbb{E}_{\theta_j, \mathcal{M}}^{\mathbb{Q}_{Y|X=x_t^{\text{test},j}}} [\mathcal{I}_q(Y)], 1 \right) \right), \quad (32)$$

with $\eta = 10^{-12}$, where $(x_1^{\text{test},j}, y_1^{\text{test},j}) \dots, (x_{n_{\text{test}}}^{\text{test},j}, y_{n_{\text{test}}}^{\text{test},j})$ denotes the test sample, and θ_j the validated hyperparameters pertaining to model \mathcal{M} , in experiment j .

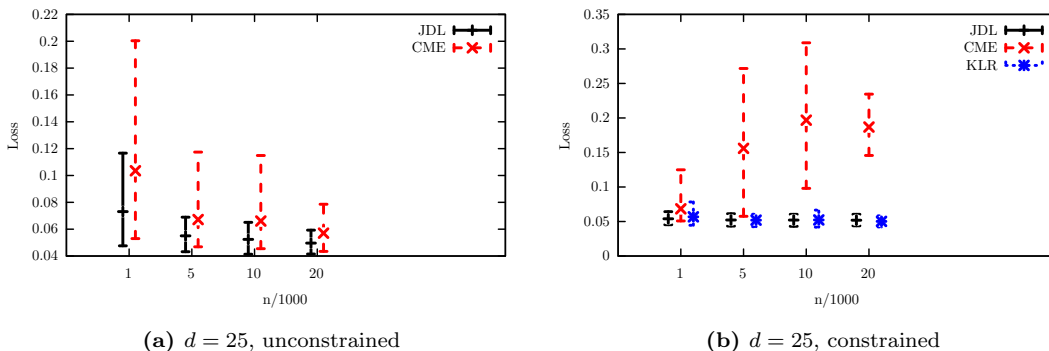


Figure 9: Logistic binary classification loss. The panels show loss function (32) evaluated over $n_{\text{test}} = 5,000$ samples for the joint distribution learner (JDL), the conditional mean embedding (CME), and logistic kernel regression (KLR) on the y -axis. The x -axis shows the number n of data points used for training and validation. The data are daily portfolio returns from Fama-French from 1927-2022.

For the JPDL, up to 26 dimensions exceed our computational means. We substitute it with a kernel logistic regression (KLR) Zhu and Hastie [2005] that is tailor-made for the task at hand, see Appendix D.

Figure 9 shows that, as for the conditional second-moment matrices, JDL dominates CME for small data sizes in the unconstrained case. In the constrained case, JDL is on par with KLR for all experiments but small sample sizes in high dimensions. The fit of CME is however severely hindered by the structural constraints.

KLR produces positive classification probabilities by construction. Figure 10 shows the estimated likelihood of generating negative classification probabilities for the other methods,

$$\frac{1}{n_{\text{test}}} \sum_{t=1}^{n_{\text{test}}} \mathbb{1} \left(\mathbb{E}_{\theta_j, \mathcal{M}}^{\mathbb{Q}_{Y|X=x_t^{\text{test},j}}} [\mathcal{I}_q(Y)] < 0 \right).$$

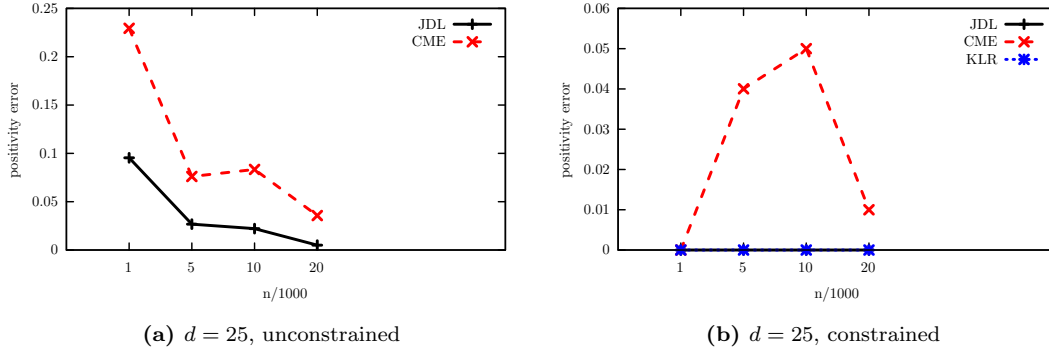


Figure 10: Logistic binary classification positivity error. The panels show the percentage of negative “probabilities” over $n_{test} = 5,000$ samples for the joint distribution learner (JDL), the conditional mean embedding (CME), and logistic kernel regression (KLR) on the y -axis. The x -axis shows the number n of data points used for training and validation. The data are daily portfolio returns from Fama-French from 1927-2022.

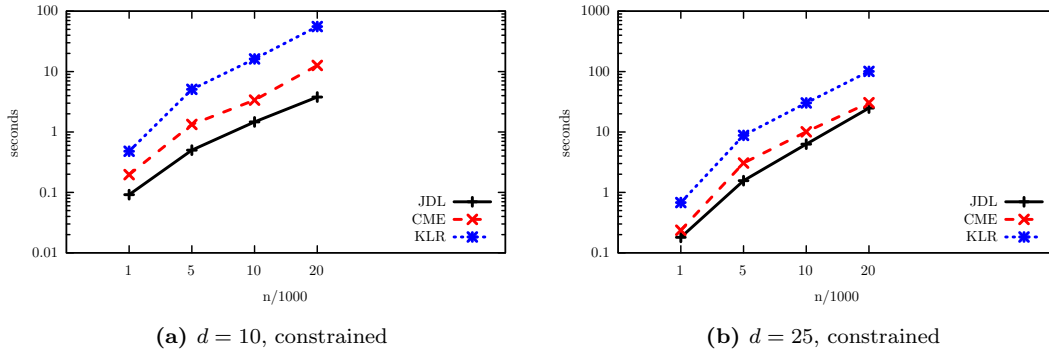


Figure 11: Logistic binary classification computation speed. The panels show the running time of calculating conditional expectations using $n_{test} = 5,000$ samples for the joint distribution learner (JDL), the conditional mean embedding (CME), and logistic kernel regression (KLR) on the y -axis. The x -axis shows the number n of data points used for training and validation. The data are daily portfolio returns from Fama-French from 1927-2022.

The structural constraints uniformly decrease the likelihood of negative probabilities in binary classification for all the methods, to zero for JDL, and two-fold to five-fold improvements for CME.

Figure 11 shows that CME and JDL are comparable in speed for the constrained case. KLR is slightly slower, but benefits greatly from its low-rank implementation. JDL thus classifies similarly well as the specialized KLR, but at greater speed.

6 Conclusion

We have proposed a new approach to estimate joint and conditional distributions in a tensor product RKHS employing adaptive low-rank approximation techniques. Our framework is well equipped to handle large samples, while satisfying positivity and normalization as important structural traits induced by probability distributions. We have shown that the presented approach is computationally efficient, versatile and successful in prediction and classification.

A Proofs

Proof of Lemma 2.1. We prove the first claim only, since the second follows similarly. In view of (4), we have

$$\mathbb{Q}_X = \frac{1}{n^2} \sum_{i,j=1}^n \delta_{x_i} + \frac{1}{n^2} \sum_{i,j=1}^n h(x_i, y_j) \delta_{x_i} = \hat{\mathbb{P}}_X + \frac{1}{n^2} \sum_{i=1}^n \left(\sum_{j=1}^n h(x_i, y_j) \right) \delta_{x_i}.$$

Hence $\mathbb{Q}_X = \hat{\mathbb{P}}_X$ is equivalent to $\frac{1}{n^2} \sum_{i=1}^n \left(\sum_{j=1}^n h(x_i, y_j) \right) \delta_{x_i} = 0$. This again holds if and only if $\sum_{i':x_{i'}=x_i} \sum_{j=1}^n h(x_{i'}, y_j) = 0$, for $i = 1, \dots, n$, as claimed. \square

Proof of Lemma 2.2. Every function f defined on \mathcal{Z} with $\sup_{z \in \mathcal{Z}} |f(z)| \leq 1$ satisfies $\|f\|_{L^2_{\hat{\mathbb{P}}_X \otimes \hat{\mathbb{P}}_Y}} \leq 1$ by the Cauchy–Schwarz inequality, and hence $\beta(\mathbb{Q}(h), \hat{\mathbb{P}}) \leq \mathcal{E}(h)^{1/2}$. As β is a metric, we have $\beta(\mathbb{Q}(h), \mathbb{P}) \leq \beta(\mathbb{Q}(h), \hat{\mathbb{P}}) + \beta(\hat{\mathbb{P}}, \mathbb{P})$, which proves the claim. \square

Proof of Theorem 3.1. First, note that for any function $h \in \mathcal{H}$ the cost function $\mathcal{E}(h)$ and the linear constraints (2) and (3) only depend on their values on the grid $h|_{\mathcal{G}}$. Denote by $\Phi_Y^\top \Phi_X: \mathcal{H} \rightarrow \mathbb{R}^{n \times n}$ the linear operator $h \mapsto h|_{\mathcal{G}}$, which evaluates h at \mathcal{G} . Hence, the image of the adjoint $(\Phi_Y^\top \Phi_X)^*$ consists of all functions of the form (10), and it is well known that its orthogonal complement in \mathcal{H} is the kernel of $\Phi_Y^\top \Phi_X$. Now, let h be any feasible function of the form (10) such that it satisfies (2) and (3). Let f be any non-zero function that is orthogonal to h in \mathcal{H} , and hence in the kernel of $\Phi_Y^\top \Phi_X$. That is, $f|_{\mathcal{G}} = \mathbf{0}$ element-wise on the grid. Then $h+f$ also satisfies (2) and (3), and $\mathcal{E}(h+f) = \mathcal{E}(h)$, while the regularized cost function is strictly greater,

$$\mathcal{E}(h+f) + \lambda \|h+f\|_{\mathcal{H}}^2 = \mathcal{E}(h) + \lambda \|h+f\|_{\mathcal{H}}^2 > \mathcal{E}(h) + \lambda \|h\|_{\mathcal{H}}^2,$$

because $\lambda > 0$. We conclude that the optimal h is of the form (10).

Expressions (11) and (12) follow by inspection. Hence (8) is equivalent to the n^2 -dimensional problem of minimizing $\mathcal{E}(h(\mathbf{H})) + \lambda \text{trace}(\mathbf{H}^\top \mathbf{K}_Y \mathbf{H} \mathbf{K}_X)$ over $\mathbf{H} \in \mathbb{R}^{n \times n}$ subject to (11) and (12). It remains to observe that this problem is equivalent to (13). Indeed, this follows because

$$\begin{aligned} & \mathcal{E}(h(\mathbf{H})) + \lambda \text{trace}(\mathbf{H}^\top \mathbf{K}_Y \mathbf{H} \mathbf{K}_X) \\ &= \frac{1}{n^2} \text{trace}[(n\mathbf{I} - \mathbf{E} - \mathbf{K}_Y \mathbf{H} \mathbf{K}_X)^\top (n\mathbf{I} - \mathbf{E} - \mathbf{K}_Y \mathbf{H} \mathbf{K}_X)] + \lambda \text{trace}(\mathbf{H}^\top \mathbf{K}_Y \mathbf{H} \mathbf{K}_X) \\ &= \mathcal{R}_\lambda(\mathbf{H}) + C, \end{aligned}$$

for a constant C that does not depend on \mathbf{H} . This completes the proof of the theorem. \square

Proof of Theorem 4.1. Without loss of generality, we assume that $p_m = m$ for $m \leq \text{rank } \mathbf{K}$. Otherwise, perform the proof with permuted matrix $\mathbf{P} \mathbf{K} \mathbf{P}^\top$ with $\mathbf{P} = [e_{p_1}, \dots, e_{p_n}]^\top$ with $\{p_{m+1}, \dots, p_n\} = \{1, \dots, n\} \setminus \{p_1, \dots, p_m\}$. The positivity of the Schur complement $\mathbf{K} - \mathbf{L}_m \mathbf{L}_m^\top$ and the error bound (15) are well known, see, for example, Harbrecht et al. [2012].

To prove the other claims, we observe that \mathbf{L}_m is a lower-triangular matrix. From line 5 in Algorithm 1, it follows that $\mathbf{b}_i \in \text{span}\{e_1, \dots, e_i\}$ for $i \leq m$, i.e., \mathbf{B}_m is upper triangular. We prove inductively that $\mathbf{B}_m^\top \mathbf{L}_m = \mathbf{I}_{m \times m}$. For $m = 1$, there holds

$$\mathbf{B}_1^\top \mathbf{L}_1 = \mathbf{b}_1^\top \ell_1 = \frac{1}{\sqrt{d_{0,1}}} e_1^\top \ell_1 = [1] = \mathbf{I}_{1 \times 1},$$

since $\ell_{1,1} = \sqrt{d_{0,1}}$. Now, let the induction hypothesis hold for $m-1$ and consider the block matrix

$$\mathbf{B}_m^\top \mathbf{L}_m = [\mathbf{B}_{m-1}, \mathbf{b}_m]^\top [\mathbf{L}_{m-1}, \ell_m] = \begin{bmatrix} \mathbf{B}_{m-1}^\top \mathbf{L}_{m-1} & \mathbf{B}_{m-1}^\top \ell_m \\ \mathbf{b}_m^\top \mathbf{L}_{m-1} & \mathbf{b}_m^\top \ell_m \end{bmatrix} \quad (33)$$

By the induction hypothesis, there holds $\mathbf{B}_{m-1}^\top \mathbf{L}_{m-1} = \mathbf{I}_{(m-1) \times (m-1)}$. Thus, since \mathbf{B}_m is upper triangular, we obtain

$$\mathbf{B}_{m-1}^\top \ell_m = \mathbf{0} \in \mathbb{R}^{(m-1) \times 1}, \quad (34)$$

and it remains to show that $\mathbf{b}_m^\top \mathbf{L}_m = \mathbf{b}_m^\top [\mathbf{L}_{m-1}, \boldsymbol{\ell}_m] = [0, \dots, 0, 1] \in \mathbb{R}^{1 \times m}$. From the induction hypothesis and (34) it follows that $\mathbf{B}_{m-1}^\top \mathbf{L}_m = [\mathbf{I}_{(m-1) \times (m-1)}, \mathbf{0}]$. Hence, we infer

$$\begin{aligned} \mathbf{b}_m^\top \mathbf{L}_m &= \frac{1}{\sqrt{d_{m-1,m}}} (\mathbf{e}_m - \mathbf{B}_{m-1} \mathbf{L}_{m-1}^\top \mathbf{e}_m)^\top \mathbf{L}_m = \frac{1}{\sqrt{d_{m-1,m}}} (\mathbf{e}_m^\top \mathbf{L}_m - \mathbf{e}_m^\top \mathbf{L}_{m-1} \mathbf{B}_{m-1}^\top \mathbf{L}_m) \\ &= \frac{1}{\sqrt{d_{m-1,m}}} \mathbf{e}_m^\top (\mathbf{L}_m - \mathbf{L}_{m-1} [\mathbf{I}_{(m-1) \times (m-1)}, \mathbf{0}]) = \frac{1}{\sqrt{d_{m-1,m}}} \mathbf{e}_m^\top [\mathbf{0}, \boldsymbol{\ell}_m]. \end{aligned}$$

In view of $\ell_{m,m} = \sqrt{d_{m-1,m}}$, we arrive at

$$\mathbf{b}_m^\top \mathbf{L}_m = \frac{1}{\sqrt{d_{m-1,m}}} \mathbf{e}_m^\top [\mathbf{0}, \boldsymbol{\ell}_m] = [0, \dots, 0, 1] \in \mathbb{R}^{1 \times m}.$$

Inserting this into (33) proves $\mathbf{B}_m^\top \mathbf{L}_m = \mathbf{I}_{m \times m}$.

With $r := \text{rank } \mathbf{K}$, we finally have

$$\mathbf{K} \mathbf{B}_m = \mathbf{L}_r \mathbf{L}_r^\top \mathbf{B}_m = \mathbf{L}_r \begin{bmatrix} \mathbf{I}_{m \times m} \\ \mathbf{0} \end{bmatrix} = \mathbf{L}_m \quad \text{for all } m \leq r.$$

This completes the proof. \square

Proof of Lemma 4.2. The claim follows from the elementary identity

$$\min_{x \in [a,b]} xy = ay^+ - by^- \quad (35)$$

for all $y \in \mathbb{R}$, for any real $a \leq b$. \square

Proof of Lemma 4.3. First, observe that the following elementary identities hold

$$\underline{\mathbf{C}}_{i,j} = \min_{s,t \in \{1, \dots, n\}} [\mathbf{L}_Y \mathbf{V}_Y]_{s,i} [\mathbf{L}_X \mathbf{V}_X]_{t,j}, \quad (36)$$

$$\overline{\mathbf{C}}_{i,j} = \max_{s,t \in \{1, \dots, n\}} [\mathbf{L}_Y \mathbf{V}_Y]_{s,i} [\mathbf{L}_X \mathbf{V}_X]_{t,j}. \quad (37)$$

Indeed, for any index pair i, j at most one of the three summands on the right hand side of (27) is different from zero, and represents the minimum if so. The same holds for the right hand side of (28) with the maximum. This proves (36) and (37).

Hence, for any index pair $s, t \in \{1, \dots, n\}$ we have

$$\begin{aligned} (\mathbf{L}_Y \mathbf{V}_Y \tilde{\mathbf{H}} \mathbf{V}_X^\top \mathbf{L}_X^\top)_{s,t} &= \sum_{i=1}^{m_Y} \sum_{j=1}^{m_X} [\mathbf{L}_Y \mathbf{V}_Y]_{s,i} \tilde{\mathbf{H}}_{i,j} [\mathbf{L}_X \mathbf{V}_X]_{t,j} \\ &\geq \sum_{i=1}^{m_Y} \sum_{j=1}^{m_X} (\underline{\mathbf{C}}_{i,j} \tilde{\mathbf{H}}_{i,j}^+ - \overline{\mathbf{C}}_{i,j} \tilde{\mathbf{H}}_{i,j}^-) = \text{trace}(\underline{\mathbf{C}}^\top \tilde{\mathbf{H}}^+) - \text{trace}(\overline{\mathbf{C}}^\top \tilde{\mathbf{H}}^-), \end{aligned}$$

where we used (35). This proves the claim. \square

Proof of Lemma 4.4. The expression on the right hand side of (30) follows from an application of the matrix derivative. Furthermore, by orthogonality of $h - h_{\tilde{\mathcal{H}}}$ and $h_{\tilde{\mathcal{H}}} - \tilde{h}$, we have

$$\|h - \tilde{h}\|_{\tilde{\mathcal{H}}}^2 = \|h - h_{\tilde{\mathcal{H}}}\|_{\tilde{\mathcal{H}}}^2 + \|h_{\tilde{\mathcal{H}}} - \tilde{h}\|_{\tilde{\mathcal{H}}}^2 = \|h - h_{\tilde{\mathcal{H}}}\|_{\tilde{\mathcal{H}}}^2 + \|\mathbf{H}_{\tilde{\mathcal{H}}} - \tilde{\mathbf{H}}\|_F^2.$$

The second equality follows from the orthonormality of $\Psi_X(\cdot)$ in \mathcal{H}_X and $\Psi_Y(\cdot)$ in \mathcal{H}_Y , see (25). It remains to bound the first term on the right hand side from above:

$$\begin{aligned}
\|h - h_{\tilde{\mathcal{H}}}\|_{\mathcal{H}}^2 &= \|\Phi_Y(\cdot)\mathbf{H}\Phi_X(\cdot)^\top - \Psi_Y(\cdot)\mathbf{H}_{\tilde{\mathcal{H}}}\Psi_X(\cdot)^\top\|_{\mathcal{H}}^2 \\
&= \|\Phi_Y(\cdot)(\mathbf{H} - \mathbf{B}_Y\mathbf{L}_Y^\top\mathbf{H}\mathbf{L}_X\mathbf{B}_X^\top)\Phi_X(\cdot)^\top\|_{\mathcal{H}}^2 \\
&= \text{trace}((\mathbf{H} - \mathbf{B}_Y\mathbf{L}_Y^\top\mathbf{H}\mathbf{L}_X\mathbf{B}_X^\top)^\top\mathbf{K}_Y(\mathbf{H} - \mathbf{B}_Y\mathbf{L}_Y^\top\mathbf{H}\mathbf{L}_X\mathbf{B}_X^\top)\mathbf{K}_X) \\
&= \text{trace}(\mathbf{H}^\top\mathbf{K}_Y\mathbf{H}\mathbf{K}_X) - 2\text{trace}(\mathbf{H}^\top\mathbf{K}_Y\mathbf{B}_Y\mathbf{L}_Y^\top\mathbf{H}\mathbf{L}_X\mathbf{B}_X^\top\mathbf{K}_X) \\
&\quad + \text{trace}(\mathbf{B}_X\mathbf{L}_X^\top\mathbf{H}^\top\mathbf{L}_Y\mathbf{B}_Y^\top\mathbf{K}_Y\mathbf{B}_Y\mathbf{L}_Y^\top\mathbf{H}\mathbf{L}_X\mathbf{B}_X^\top\mathbf{K}_X) \\
&= \text{trace}(\mathbf{H}^\top\mathbf{K}_Y\mathbf{H}\mathbf{K}_X) - \text{trace}(\mathbf{H}^\top\mathbf{L}_Y\mathbf{L}_Y^\top\mathbf{H}\mathbf{L}_X\mathbf{L}_X^\top) \\
&= \text{trace}(\mathbf{H}^\top\mathbf{K}_Y\mathbf{H}(\mathbf{K}_X - \mathbf{L}_X\mathbf{L}_X^\top)) + \text{trace}(\mathbf{H}^\top(\mathbf{K}_Y - \mathbf{L}_Y\mathbf{L}_Y^\top)\mathbf{H}\mathbf{L}_X\mathbf{L}_X^\top) \\
&= \langle \mathbf{K}_Y, \mathbf{H}(\mathbf{K}_X - \mathbf{L}_X\mathbf{L}_X^\top)\mathbf{H}^\top \rangle_F + \langle \mathbf{L}_X\mathbf{L}_X^\top, \mathbf{H}^\top(\mathbf{K}_Y - \mathbf{L}_Y\mathbf{L}_Y^\top)\mathbf{H} \rangle_F \\
&\leq \|\mathbf{H}\|_F^2\|\mathbf{K}_Y\|_F\|\mathbf{K}_X - \mathbf{L}_X\mathbf{L}_X^\top\|_F + \|\mathbf{H}\|_F^2\|\mathbf{L}_X\mathbf{L}_X^\top\|_F\|\mathbf{K}_Y - \mathbf{L}_Y\mathbf{L}_Y^\top\|_F \\
&\leq \varepsilon\|\mathbf{H}\|_F^2(\text{trace}\mathbf{K}_X + \text{trace}\mathbf{K}_Y),
\end{aligned}$$

where we used the Cauchy–Schwarz inequality for the Frobenius inner product, as well as the sub-multiplicativity of the Frobenius norm, and the fact that $\|\mathbf{A}\|_F \leq \text{trace}\mathbf{A}$ for any positive semidefinite matrix \mathbf{A} , and $\text{trace}\mathbf{L}_X\mathbf{L}_X^\top \leq \text{trace}\mathbf{K}_X$. \square

B Polynomial distributions

Finite-dimensional RKHS lead to low-rank problems by construction, and in this section, we specialize our approach to polynomial kernels that are particularly amenable to positivity constraints. In this setting, the rank of the kernel matrices is predetermined from the degree of the polynomial, and does not necessitate additional low-rank techniques, as described in the previous section for large data sets. Furthermore, as we will see below, the polynomial kernel basis with a particularly suitable inner product is automatically double-orthogonal, without requiring further modifications or rotations.

Let $\mathcal{X} \subseteq \mathbb{R}^{d_X}$ and $\mathcal{Y} \subseteq \mathbb{R}^{d_Y}$, with non-empty interiors, and choose a common polynomial degree q for simplicity. Let $\mathcal{P}_q(\mathcal{X}) := \text{span}\{x^\alpha : \alpha \in \mathbb{N}^{d_X}, |\alpha| \leq q\}$ and $\mathcal{P}_q(\mathcal{Y}) := \text{span}\{y^\alpha : \alpha \in \mathbb{N}^{d_Y}, |\alpha| \leq q\}$, denote the spaces of all polynomials on \mathcal{X} and \mathcal{Y} of degree q or less. The dimensions of the vectors of monomials generating $\mathcal{P}_q(\mathcal{X})$ and $\mathcal{P}_q(\mathcal{Y})$, $\tau_{X,q}(x) := [\tau_{X,q,1}(x), \dots, \tau_{X,q,m_X}(x)]$, and $\tau_{Y,q}(y) := [\tau_{Y,q,1}(y), \dots, \tau_{Y,q,m_Y}(y)]$, are $m_X = \binom{d_X+q}{d_X}$ and $m_Y = \binom{d_Y+q}{d_Y}$, respectively.

To use these polynomial bases in the context of loss function (14), we use expectation inner products in terms of $\hat{\mathbb{P}}_X$ and $\hat{\mathbb{P}}_Y$, respectively. Assuming that the Gram matrices

$$\mathbf{G}_{X,q} := \left[\int_{\mathcal{X}} \tau_{X,q,i} \tau_{X,q,j} d\hat{\mathbb{P}}_X \right]_{i,j=1}^n \quad \text{and} \quad \mathbf{G}_{Y,q} := \left[\int_{\mathcal{Y}} \tau_{Y,q,i} \tau_{Y,q,j} d\hat{\mathbb{P}}_Y \right]_{i,j=1}^n,$$

have full rank, we define the kernels $k_{X,q} : \mathcal{X} \times \mathcal{X} \mapsto \mathbb{R}$ and $k_{Y,q} : \mathcal{Y} \times \mathcal{Y} \mapsto \mathbb{R}$ by

$$k_{X,q}(x, x') = \tau_{X,q}(x)\mathbf{G}_{X,q}^{-1}\tau_{X,q}^\top(x') \quad \text{and} \quad k_{Y,q}(y, y') = \tau_{Y,q}(y)\mathbf{G}_{Y,q}^{-1}\tau_{Y,q}^\top(y').$$

For details on polynomial kernels, we refer to [Berlinet and Thomas-Agnan \[2004\]](#). Defining the Vandermonde matrices

$$\mathbf{V}_{X,q} := \begin{bmatrix} \tau_{X,q}(x_1) \\ \vdots \\ \tau_{X,q}(x_n) \end{bmatrix}, \quad \text{and} \quad \mathbf{V}_{Y,q} := \begin{bmatrix} \tau_{Y,q}(y_1) \\ \vdots \\ \tau_{Y,q}(y_n) \end{bmatrix},$$

the corresponding kernel matrices have natural decompositions,

$$\mathbf{K}_X = \mathbf{V}_{X,q}\mathbf{G}_{X,q}^{-1/2}\mathbf{G}_{X,q}^{-1/2}\mathbf{V}_{X,q}^\top = \mathbf{L}_X\mathbf{L}_X^\top \quad \text{and} \quad \mathbf{K}_Y = \mathbf{V}_{Y,q}\mathbf{G}_{Y,q}^{-1/2}\mathbf{G}_{Y,q}^{-1/2}\mathbf{V}_{Y,q}^\top = \mathbf{L}_Y\mathbf{L}_Y^\top.$$

These decompositions correspond to the orthogonal bases $\tau_{X,q} \mathbf{G}_{X,q}^{-1/2}$ and $\tau_{Y,q} \mathbf{G}_{Y,q}^{-1/2}$, respectively. Especially, for either kernel matrix we have $\mathbf{L}_X^\top \mathbf{L}_X = \mathbf{L}_Y^\top \mathbf{L}_Y = n\mathbf{I}$, immediately identifying

$$\mathbf{B}_X = \mathbf{L}_X/n \text{ and } \mathbf{B}_Y = \mathbf{L}_Y/n,$$

which satisfy the requirements (15)–(18) with tolerance $\varepsilon = 0$, as well as double orthogonality in both \mathcal{H} and $L_{\hat{\mathbb{P}}_X \otimes \hat{\mathbb{P}}_Y}^2$, without further modifications.

Having provided the necessary ingredients, and setting $\mathbf{H} = \mathbf{B}_Y \tilde{\mathbf{H}} \mathbf{B}_X^\top = \frac{1}{n^2} \mathbf{L}_Y \tilde{\mathbf{H}} \mathbf{L}_X^\top$, the objective function (14) simplifies to

$$(1 + \lambda) \text{trace}(\tilde{\mathbf{H}}^\top \tilde{\mathbf{H}}) - \frac{2}{n} \text{trace}(\mathbf{L}_Y \tilde{\mathbf{H}} \mathbf{L}_X^\top) + \frac{2}{n^2} \text{trace}(\mathbf{1}^\top \mathbf{L}_Y \tilde{\mathbf{H}} \mathbf{L}_X^\top \mathbf{1}). \quad (38)$$

On top of their innate low-rank nature, polynomials grant one additional advantage in that they lend themselves to a tightening of the positivity (3) on the grid \mathcal{G} to a global pointwise positivity condition. From the tensor product space $\mathcal{H} = \mathcal{P}_q(\mathcal{X}) \otimes \mathcal{P}_q(\mathcal{Y}) \subset \mathcal{P}_{2q}(\mathcal{Z})$, we define

$$\mathcal{P}_{\text{sos},2q}(\mathcal{Z}) := \{\xi \in \mathcal{P}_{2q}(\mathcal{Z}) : \xi = \tau_q \mathbf{A} \tau_q^\top \text{ with } \mathbf{A} \succeq 0\}, \quad (39)$$

the sum-of-squares cone of degree $2q$ polynomials on \mathcal{Z} , where τ_q here denotes the basis monomials in z of degree q or less.² Through the tensor product formulation, global pointwise positivity can in the polynomial case thus be ensured through the semidefinite constraint $1+h \in \mathcal{P}_{\text{sos},2q}(\mathcal{Z})$.

C Conditional Mean Embedding

Here, we introduce briefly conditional mean embedding as proposed by Song et al. [2009], who employ the same hypothesis space, a tensor product RKHS $\mathcal{H} = \mathcal{H}_X \otimes \mathcal{H}_Y$, that is used in the previous sections to estimate, for any $x \in \mathcal{X}$, the conditional expectation operator $\mu_{Y|X=x} \in \mathcal{H}_Y$ acting as a linear functional on \mathcal{H}_Y

$$\langle f, \mu_{Y|X=x} \rangle_{\mathcal{H}_Y} = \int_{\mathcal{Y}} f \, d\mathbb{P}_{Y|X=x}, \quad \text{for all } f \in \mathcal{H}_Y. \quad (40)$$

Consider a sample (x_i, y_i) , $i = 1, \dots, n$ as above. Assuming that there exists an element $\mu_{Y|X=..} \in \mathcal{H}$ satisfying (40) for all $x \in \mathcal{X}$, Grünewälder et al. [2012] show that among $F: \mathcal{X} \mapsto \mathcal{H}_Y$, $F \in \mathcal{H}$, the best estimator is given by

$$\hat{\mu}_{Y|X=..} := \arg \min_{F \in \mathcal{H}} \left\{ \frac{1}{n} \sum_{i=1}^n \|k_{\mathcal{Y}}(y_i, \cdot) - F(x_i)\|_{\mathcal{H}_Y}^2 + \lambda \|F\|_{\mathcal{H}}^2 \right\}. \quad (41)$$

Note, however, that the validity of this assumption is difficult to test in practice, as discussed, for example, in Klebanov et al. [2020].

Leaving aside these difficulties, the optimal F in (41) is found to be of the form $F = \Phi_Y(\cdot) \mathbf{F} \Phi_X(\cdot)^\top$, where $\Phi_Y(\cdot)$ and $\Phi_X(\cdot)$ are given as in (9), which follows from Micchelli and Pontil [2005]. With this bilinear form, solving (41) thus yields the solution

$$\mathbf{F} = (\mathbf{K}_X + n\lambda \mathbf{I}_n)^{-1}, \quad \text{and } \hat{\mu}_{Y|X=..} = \Phi_Y(\cdot) (\mathbf{K}_X + n\lambda \mathbf{I}_n)^{-1} \Phi_X(\cdot)^\top. \quad (42)$$

The estimator of the conditional expectation operator (40) then reads

$$\langle f, \hat{\mu}_{Y|X=x} \rangle_{\mathcal{H}_Y} = [f(y_1), \dots, f(y_n)] \mathbf{F} \Phi_X^\top(x), \quad \text{for all } f \in \mathcal{H}_Y. \quad (43)$$

From (43), it is noteworthy, that the optimal conditional mean embedding does not feature the kernel matrix \mathbf{K}_Y . The RKHS \mathcal{H}_Y appears only to evaluate functions. However, working with large data sets becomes prohibitive, due to the matrix inversion in (42).

²Sum-of-square positivity constraints are tightly related to the moment problem Lasserre [2010], Schmüdgen [2017], and have been prominent also in machine learning Muzellec et al. [2021].

C.1 Low-rank approximation of the Conditional Mean Embedding

To facilitate low-rank approximations as in Section 4, we first need to develop the objective function. Multiplying the objective function with n and omitting the term that does not depend on \mathbf{F} , we can write the objective function (41) as

$$\begin{aligned} \mathcal{R}_\lambda^{\text{CME}}(\mathbf{F}) &:= \sum_{i=1}^n \{-2\Phi_Y(y_i) \mathbf{F} \Phi_X^\top(x_i) + \Phi_X^\top(x_i) \mathbf{F}^\top \mathbf{K}_Y \mathbf{F} \Phi_X^\top(x_i)\} \\ &\quad + n\lambda \text{trace}(\mathbf{F}^\top \mathbf{K}_Y \mathbf{F} \mathbf{K}_X) \\ &= -2 \text{trace}(\mathbf{K}_Y \mathbf{F} \mathbf{K}_X) + \text{trace}(\mathbf{F}^\top \mathbf{K}_Y \mathbf{F} \mathbf{K}_X \mathbf{K}_X) + n\lambda \text{trace}(\mathbf{F}^\top \mathbf{K}_Y \mathbf{F} \mathbf{K}_X) \\ &= -2 \text{trace}(\mathbf{K}_Y \mathbf{F} \mathbf{K}_X) + \text{trace}(\mathbf{F}^\top \mathbf{K}_Y \mathbf{F} \mathbf{K}_X (\mathbf{K}_X + n\lambda \mathbf{I}_n)). \end{aligned} \quad (44)$$

From the first order condition of optimality with respect to the matrix \mathbf{F} , the solution (42) evolves from this objective function in coordinate form.³

The proposal in Grünwaldler et al. [2012] to sparsify conditional mean embedding necessitates the calculation of the full kernel matrix \mathbf{K}_X , which may become prohibitive for large sample sizes. To avoid calculations with large matrices, we consider a proposal following the low-rank Section 4. Inserting

$$\mathbf{F} = \mathbf{B}_Y \mathbf{V}_Y \tilde{\mathbf{F}} \mathbf{V}_X^\top \mathbf{B}_X^\top \quad (45)$$

into the objective function (44), for $\tilde{\mathbf{F}} \in \mathbb{R}^{m_Y \times m_X}$, we obtain the low-rank objective function on $\mathbb{R}^{m_Y \times m_X}$

$$\begin{aligned} \tilde{\mathcal{R}}_\lambda^{\text{CME}}(\tilde{\mathbf{F}}) &:= \mathcal{R}_\lambda^{\text{CME}}(\mathbf{B}_Y \mathbf{V}_Y \tilde{\mathbf{F}} \mathbf{V}_X^\top \mathbf{B}_X^\top) \\ &= -2 \text{trace}(\mathbf{L}_Y \mathbf{V}_Y \tilde{\mathbf{F}} \mathbf{V}_X^\top \mathbf{L}_X^\top) + \text{trace}(\tilde{\mathbf{F}} \mathbf{\Lambda}_X \tilde{\mathbf{F}}^\top + n\lambda \tilde{\mathbf{F}} \tilde{\mathbf{F}}^\top). \end{aligned} \quad (46)$$

To work with the optimal solution (42) without low-rank approximation, one never has to make explicit \mathcal{H}_Y . One rather merely assumes that it can always be specified to accommodate the functions to be evaluated therein. In the low-rank objective function (46) the low-rank kernel matrix does appear, however. As a consequence function evaluation is also performed only on the reduced subspace. We refer to the low-rank conditional mean embedding as CME.

C.2 Structural constraints for the Conditional Mean Embedding

Similarly to the distribution estimator proposed in this paper, and assuming there exists $f \in \mathcal{H}_Y$ with $f(y_i) = 1$ for $i = 1, \dots, n$, we can impose normalization of the conditional distributions as the n vector constraint

$$\mathbf{1}^\top \mathbf{F} \mathbf{K}_X = \mathbf{1}^\top \mathbf{B}_Y \mathbf{V}_Y \tilde{\mathbf{F}} \mathbf{V}_X^\top \mathbf{L}_X^\top = \mathbf{1}^\top. \quad (47)$$

Likewise, assuming that there exist $f_1, \dots, f_n \in \mathcal{H}_Y$ such that $f_i(y_j) = \delta_{ij}$ for $i, j = 1, \dots, n$, positivity can be imposed as the $n \times n$ matrix inequality

$$\mathbf{F} \mathbf{K}_X = \mathbf{B}_Y \mathbf{V}_Y \tilde{\mathbf{F}} \mathbf{V}_X^\top \mathbf{L}_X^\top \geq \mathbf{0}_{n \times n}, \text{ element-wise.} \quad (48)$$

Note that only the m_Y non-zero rows $p_{Y,1}, \dots, p_{Y,m_Y}$ of \mathbf{B}_Y in (48) are relevant. Hence the effective dimension of (48) is significantly smaller than $n \times n$. We therefore define the $m_Y \times n$ matrix

$$\tilde{\mathbf{B}}_Y := \mathbf{P}_Y^\top \mathbf{B}_Y,$$

consisting of the m_Y non-zero rows $p_{Y,1}, \dots, p_{Y,m_Y}$ of \mathbf{B}_Y , for the $n \times m_Y$ matrix $\mathbf{P}_Y := (\mathbf{e}_{p_{Y,1}}, \dots, \mathbf{e}_{p_{Y,m_Y}})$. We then replace (48) by the equivalent $m_Y \times n$ matrix condition

$$\tilde{\mathbf{B}}_Y \mathbf{V}_Y \tilde{\mathbf{F}} \mathbf{V}_X^\top \mathbf{L}_X^\top \geq \mathbf{0}_{m_Y \times n}, \text{ element-wise.} \quad (49)$$

³Taking the matrix derivative of (44) with respect to \mathbf{F} , yields the condition

$$-2\mathbf{K}_Y \mathbf{K}_X + 2\mathbf{K}_Y \mathbf{F} (\mathbf{K}_X + n\lambda \mathbf{I}_n) \mathbf{K}_X = \mathbf{0},$$

from which it becomes apparent how the solution is independent of \mathbf{K}_Y at the optimum.

Putting everything together, constrained low-rank CME solves the program

$$\underset{\tilde{\mathbf{F}} \in \mathbb{R}^{m_Y \times m_X} \text{ s.t. (47), (49)}}{\text{minimize}} \quad \tilde{\mathcal{R}}_\lambda^{\text{CME}}(\tilde{\mathbf{F}}). \quad (50)$$

There are two major computational issues for the implementation of (50). First, the normalization constraint (47) imposes n linear restrictions, which will likely be infeasible, in particular for large n compared to the dimension $m_X m_Y$ of the argument $\tilde{\mathbf{F}}$. We therefore significantly weaken this linear constraint, and impose normalization only for the unconditional mean equivalent

$$\mathbf{1}^\top \mathbf{B}_Y \mathbf{V}_Y \tilde{\mathbf{F}} \mathbf{V}_X^\top \mathbf{L}_X^\top \mathbf{1} / n = 1. \quad (51)$$

Second, for large n , the positivity constraint (49) becomes computationally difficult. A tightening along the lines of (29) turns out to be infeasible in our numerical examples. An alternative is the relaxation of the positivity constraint (49), which is similar to (51), namely the unconditional positivity constraint

$$\tilde{\mathbf{B}}_Y \mathbf{V}_Y \tilde{\mathbf{F}} \mathbf{V}_X^\top \mathbf{L}_X^\top \mathbf{1} \geq \mathbf{0}_{m_Y}, \text{ element-wise.} \quad (52)$$

D Kernel logistic regression

We employ the standard kernelized classifier for a coefficient vector $\mathbf{c} \in \mathbb{R}^n$, $\text{cl}(\cdot) := (1 + \exp(-\Phi_X(\cdot)\mathbf{c}))^{-1}$, and mapping

$$x \mapsto \begin{cases} 1, & \text{cl}(x) \geq 1/2, \\ 0, & \text{cl}(x) < 1/2. \end{cases}$$

Applying the transformation $\mathbf{c} = \mathbf{B}_X \tilde{\mathbf{c}}$, and defining $\tilde{\Phi}_X(\cdot) := \Phi_X(\cdot)\mathbf{B}_X$ yields the low-rank classifier $\tilde{\text{cl}}(\cdot) = (1 + \exp(-\tilde{\Phi}_X(\cdot)\tilde{\mathbf{c}}))^{-1}$. With regularization, the optimal coefficients minimizing the logistic loss, as in (32), solve

$$\underset{\tilde{\mathbf{c}} \in \mathbb{R}^{m_X}}{\text{minimize}} \left\{ - \sum_{i=1}^n \mathcal{I}_q(y_i) \log \tilde{\text{cl}}(x_i) - \sum_{i=1}^n (1 - \mathcal{I}_q(y_i)) \log (1 - \tilde{\text{cl}}(x_i)) + \lambda \|\tilde{\mathbf{c}}\|_2^2 \right\},$$

for $\lambda > 0$, where we have made use of bi-orthogonality in the regularization.

References

- Amirhesam Abedsoltan, Mikhail Belkin, and Parthe Pandit. Toward large kernel models. In *International Conference on Machine Learning*, pages 61–78. PMLR, 2023. 7
- Ilya Archakov and Peter Reinhard Hansen. A new parametrization of correlation matrices. *Econometrica*, 89(4):1699–1715, 2021. 10, 11, 12, 13, 14
- F.R. Bach and M.I. Jordan. Kernel independent component analysis. *Journal of Machine Learning Research*, 3(Jul):1–48, 2002. 2
- N.H.F. Beebe and J. Linderberg. Simplifications in the generation and transformation of two-electron integrals in molecular calculations. *International Journal of Quantum Chemistry*, 12(4):683–705, 1977. 2
- Alain Berlinet and Christine Thomas-Agnan. *Reproducing Kernel Hilbert Spaces in Probability and Statistics*, pages 1–54. Springer US, Boston, MA, 2004. 1, 19
- R. M. Dudley. *Real analysis and probability*, volume 74 of *Cambridge Studies in Advanced Mathematics*. Cambridge University Press, Cambridge, 2002. ISBN 0-521-00754-2. Revised reprint of the 1989 original. 3, 4

- Richard Mansfield Dudley. The speed of mean glivenko-cantelli convergence. *The Annals of Mathematical Statistics*, 40(1):40–50, 1969. 4
- L. Foster, A. Waagen, N. Aijaz, M. Hurley, A. Luis, J. Rinsky, C. Satyavolu, and M. Com. Stable and Efficient Gaussian Process Calculations. *Journal of Machine Learning Research*, 10:857–882, 2009. 2
- Kenji Fukumizu, Francis R. Bach, and Michael I. Jordan. Dimensionality reduction for supervised learning with reproducing kernel hilbert spaces. *Journal of Machine Learning Research*, 5: 73–99, dec 2004. ISSN 1532-4435. 1
- U. Grenander. *Abstract inference / Ulf Grenander*. Wiley New York, 1981. 1
- S. Grünewälder, G. Lever, L. Baldassarre, S. Patterson, A. Gretton, and M. Pontil. Conditional mean embeddings as regressors. In *Proceedings of the 29th International Conference on Machine Learning*, pages 1823–1830, New York, 2012. Omnipress. 1, 6, 9, 20, 21
- H. Harbrecht, M. Peters, and R. Schneider. On the low-rank approximation by the pivoted Cholesky decomposition. *Applied Numerical Mathematics*, 62:28–440, 2012. 2, 6, 17
- Nicholas J. Higham. *Accuracy and Stability of Numerical Algorithms*. Society for Industrial and Applied Mathematics, Philadelphia, 1996. 6
- Ilya Klebanov, Ingmar Schuster, and T. J. Sullivan. A rigorous theory of conditional mean embeddings. *SIAM Journal on Mathematics of Data Science*, 2(3):583–606, 2020. 1, 2, 20
- Jean Bernard Lasserre. *Moment, Positive Polynomials and Their Applications*, volume 1 of *Imperial College Press Optimization Series*. Imperial College Press, 2010. 20
- Qi Li and Jeffrey Scott Racine. *Nonparametric Econometrics: Theory and Practice*, volume 1 of *Economics Books*. Princeton University Press, 2006. 1
- Giacomo Meanti, Luigi Carratino, Lorenzo Rosasco, and Alessandro Rudi. Kernel methods through the roof: handling billions of points efficiently. *Advances in Neural Information Processing Systems*, 33:14410–14422, 2020. 7
- Charles A. Micchelli and Massimiliano A. Pontil. On learning vector-valued functions. *Neural Computation*, 17(1):177–204, 2005. 1, 20
- Boris Muzellec, Francis Bach, and Alessandro Rudi. A note on optimizing distributions using kernel mean embeddings. *arXiv:2106.09994*, 2021. 2, 20
- XuanLong Nguyen, Martin J. Wainwright, and Michael I. Jordan. Estimating divergence functionals and the likelihood ratio by convex risk minimization. *IEEE Transactions on Information Theory*, 56(11):5847–5861, 2010. 2
- Junhyung Park and Krikamol Muandet. A measure-theoretic approach to kernel conditional mean embeddings. In *Proceedings of the 34th International Conference on Neural Information Processing Systems*, NIPS’20, Red Hook, NY, USA, 2020. Curran Associates Inc. ISBN 9781713829546. 1
- Konrad Schmüdgen. *The Moment Problem*. Graduate Texts in Mathematics. Springer International Publishing, 2017. ISBN 9783319645469. URL <https://books.google.ch/books?id=nuO9DwAAQBAJ>. 20
- Ingmar Schuster, Mattes Mollenhauer, Stefan Klus, and Krikamol Muandet. Kernel conditional density operators. In Silvia Chiappa and Roberto Calandra, editors, *Proceedings of the 23rd International Conference on Artificial Intelligence and Statistics (AISTATS) 2020*, volume 108 of *Proceedings of Machine Learning Research*, pages 993–1004, Online, 26–28 Aug 2020. PMLR. 2

- Alex Smola, Arthur Gretton, Le Song, and Bernhard Schölkopf. A hilbert space embedding for distributions. In Marcus Hutter, Rocco A. Servedio, and Eiji Takimoto, editors, *Algorithmic Learning Theory*, pages 13–31, Berlin, Heidelberg, 2007. Springer Berlin Heidelberg. ISBN 978-3-540-75225-7. [1](#)
- Le Song, Jonathan Huang, Alex Smola, and Kenji Fukumizu. Hilbert space embeddings of conditional distributions with applications to dynamical systems. In *Proceedings of the 26th Annual International Conference on Machine Learning, ICML 2009*, pages 961–968, New York, 2009. Association for Computing Machinery. ISBN 9781605585161. [1](#), [9](#), [20](#)
- Le Song, Kenji Fukumizu, and Arthur Gretton. Kernel embeddings of conditional distributions: A unified kernel framework for nonparametric inference in graphical models. *IEEE Signal Processing Magazine*, 30(4):98–111, 2013. [1](#)
- Holger Wendland. *Scattered Data Approximation*. Cambridge University Press, Cambridge, 2005. [3](#)
- Christopher Williams and Matthias Seeger. Using the Nyström method to speed up kernel machines. In T. Leen, T. Dietterich, and V. Tresp, editors, *Advances in Neural Information Processing Systems*, volume 13. MIT Press, 2000. [6](#)
- Ji Zhu and Trevor Hastie. Kernel logistic regression and the import vector machine. *Journal of Computational and Graphical Statistics*, 14(1):185–205, 2005. [15](#)